LUND UNIVERSITY

LTH

FACULTY OF ENGINEERING

A Parametric Study of Mirrorless Lasing Dynamics

Klara Lozani Gerdhem

Thesis submitted for the degree Master in Photonics

Project duration: 4.5 months

Supervised by: Prof. Joakim Bood, Ass. Prof. Andreas Ehn, Dr. Vassily Kornienko, and Dr. Jonas Ravelid

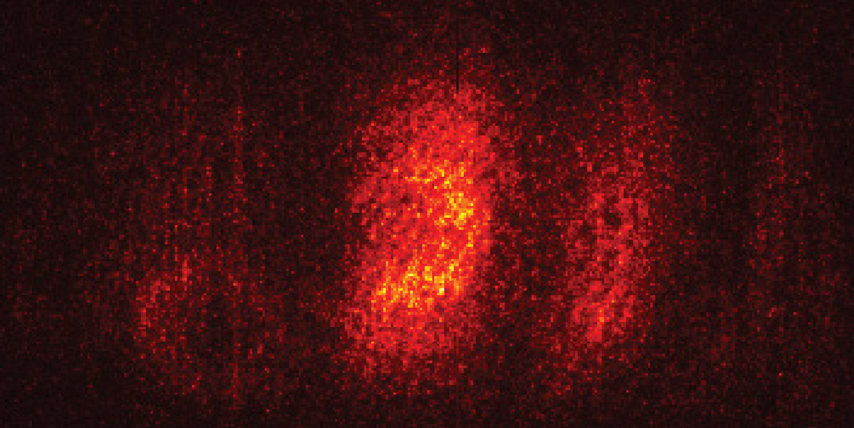

Department of Physics, Division of Combustion Physics, June 2026

A Parametric Study of Mirrorless Lasing Dynamics

by Klara Lozani Gerdhem

Thesis submitted for the degree Master of Science, Photonics
Project duration: Nine months at half-speed
Thesis advisors: Prof. Joakim Bood, Ass. Prof. Andreas Ehn, Dr. Vassily Kornienko, and Dr. Jonas Ravelid
Division of Combustion Physics

Abstract

There exists a lack of laser-based remote sensing methods that give signals with high intensity and directionality. According to previous research, mirrorless lasing can meet these requirements; however, neither the dependence on the gain medium geometry nor the light-matter interaction responsible for the emission has been investigated in detail. This thesis project examined the sideways lasing emission from a gain medium with a Fresnel number $F \ll 1$, generated by the overlap of two counterpropagating femtosecond laser pulses in xenon gas at atmospheric pressure. Both spatial and temporal measurements of the sideways lasing emission were made, with the latter being obtained using a streak camera. The emission was highly localised in space, suggesting it originated from the overlap. It also yielded a power dependence with a clear threshold and an interference pattern indicating coherence, both of which showed strong agreement with the predicted behaviour for superfluorescence (SF). The recorded temporal profile displayed a pulse with oscillations on the incline and the decline, appearing with a delay of about 70 ps relative to the excitation pulse and thus corresponding well to the theoretical predictions for SF emitted from a gain medium with $F \ll 1$. It can therefore be concluded that the observed sideways lasing was generated by SF. Additionally, the dependence of the emission on the gain medium geometry was in good accordance with theory. These measurements, to the best of the author's knowledge, provide the first thorough investigation of mirrorless lasing at atmospheric pressure for this gain medium configuration, thus opening the way for both further fundamental research and the implementation of these techniques in applied laser diagnostics.

Acknowledgments

Firstly, I would like to begin by thanking my main supervisors, Joakim Bood and Andreas Ehn. Joakim, your expert knowledge and never-ending interest in the field are both very impressive and so very inspiring. Thank you for always having time to answer a question and for always taking the time to discuss the most interesting physics there is. Andreas, your positive personality and endless ideas have motivated me to always take my experiments one step further and to never stop approaching research with great optimism. Thank you both for supporting me in all of these extremely cool experiments!

Now onto my co-supervisors, Vasse and Jonas. Vasse, where should I even start? Not only did you guide me during the experimental seminars, but also during my bachelor's thesis, various research projects, and now my master's thesis. Your amazing personality and love for physics have always motivated and inspired me. Your help has truly been priceless - many of the wonderful experimental results are in this thesis, much thanks to you. So, seriously, thank you for everything. Jonas, you are the one who convinced me to do this project, so it is definitely true that this thesis would not exist without you! Thank you for both coming up with crazy and oh-so-cool ideas, but also for always being there whenever I needed support. I am so grateful to you for teaching me about some of the most interesting things I have ever studied. I will miss working with both of you so much - but I am also sure that this was not the last time!

Continuing with the best division at Lund University - The Division of Combustion Physics. Thank you all for making this the best workplace. To the people in the student office, Saga, Dorota, Hugo, and Claire, thank you for this year and for all the fun times that we have shared! To my opponents, Olivia and Hilma, thank you for taking the time to read this thesis. But more importantly, thank you for our wonderful morning walks and for always being there to talk about anything. I have so cherished our discussions, teamwork, and friendship during these last 1.5 years - it has truly been a wonderful time!

To my two best friends, Sara and Benji. You guys are just simply the best. Sara, thank you for being the most amazing friend during these last 7(!) years. You are such a wonderful person and so incredibly talented. I look forward to us reminiscing about our student years and drinking tea in our eighties! Benji, thank you for being the best friend a girl could ask for. Thank you for listening to all my rants, supporting me every single time, and for the most fun times ever!

Mamma och pappa, tack för att ni är de bästa föräldrarna som det bara går att få. Jag hade definitivt inte suttit här och skrivit detta idag om jag inte hade haft ert otroliga stöd under alla mina 25 levnadsår. Tack för att ni alltid, alltid har trott på mig till 100%. Pappa, tack för att du har inspirerat mig till att jobba med något som jag älskar. Mamma, tack för att du lärde mig att flyga i tanken – det är mycket tack vare det att jag snart ska ta masterexamen i fysik.

Max, the love of my life, my happiness, my everything. I will never stop being grateful for having you in my life. Thank you for your eternal support and love - with this, I feel like I can do anything!

Popular summary

Imagine a world where we could get information about objects many meters away without having to get close to them. Maybe that object is something we disturb if we get too close, like an insect, or something dangerous, like rocket exhaust. We can actually do things like this today, using lasers. Usually, the researchers then send laser light to the object, which absorbs it and emits another type of light. The type of light we get back depends on the object, since objects react differently to different types of light. This means that if the researchers detect this light, it will give them a lot of very useful information about the object.

There is one big problem, though - the light sent back from the object is usually very weak, since it spreads out in all directions. This makes it very difficult to detect, making the extracted information unreliable. Sadly, this limits modern research, since some experiments just become too difficult to perform. The purpose of this project is to solve this problem. We want to investigate an unknown type of light called mirrorless lasing. This light has a clear direction, making it much easier to detect and making the signal effectively stronger. In many ways, this light is similar to that from a laser, but we do not need mirrors or any other parts of a laser to create it (which explains the name). The only problem is that there are in fact very few academic studies aimed at understanding this form of light in an experimental setting, even so that what is presented herein has never been done. However, we want to take it one step further, and also investigate if we can control the direction that this light is sent out in.

When an atom gets in contact with a laser, it can sometimes absorb this light. Since light can be seen as energy, this absorption will excite it to a higher energy state. This level will always be unstable, so the atom will return to its initial state after a certain time. It then loses the energy it gained before, and now this energy has to go somewhere. One way for the atom to get rid of the energy is to send it out as light again. The amount of light emitted will then correspond exactly to the energy jump that the atom made, meaning that the light automatically will carry information about that specific atom. This energy jump can occur through many different physical processes, which give the light different properties. Generally, there are two main categories of emitted light. Most of it behaves as the sun, meaning that it is sent out equally in every single direction. Then there is a smaller category in which the light behaves like a laser, emitting a narrow beam with a clear direction. Mirrorless lasing falls into the second category, and it is even more interesting because it is so little investigated. Which type of light that is emitted depends on several factors - the intensity of the laser exciting the atoms, how long they are in contact with the laser, how many atoms we have, and which type of atoms we have, to name a few.

But how do we then generate this rare form of light that we call mirrorless lasing? This is done by focusing the laser beam into a gas. The atoms in the focus will absorb most of the light, and only they will emit the mirrorless lasing. When we have created the light, we can see how it travels through space and in time. Then we can take all this information and compare it with all known physical processes that generate light to see which one best matches our observations.

Previous research on mirrorless lasing showed that how the laser beam is focused will determine the direction that the light is emitted in. We wanted to easily compare theory to our experiment, so we chose a focus geometry that was well predicted: an extremely thin line. To get this, it is not enough to simply focus the laser beam. We need to use a pulsed laser that sends two laser pulses in opposite directions. Where these two pulses meet in space and time, the intensity from the laser will be twice as high as everywhere else where the laser pulses pass. The mirrorless lasing will then be emitted only from the region where the pulses overlap, which is extremely thin for an ultrafast laser.

To summarise, this project aims to learn more about an unknown type of emission that will drive research forward. The more we learn about mirrorless lasing, the more we can use it. This project will then take us one step closer to a future where we can create laser-like light using nothing but light itself.

Abbreviations

TDSE	**T**ime-**D**ependent **S**chrödinger **E**quation
FWHM	**F**ull **W**idth **H**alf-**M**aximum
ASE	**A**mplified **S**pontaneous **E**mission
SF	**S**uper**f**luorescence
LIF	**L**aser-**I**nduced **F**luorescence
TALIF	**T**wo-photon **A**bsorption **L**aser-**I**nduced **F**luorescence
VUV	**V**acuum **U**ltra**v**iolet

Table of Contents

1 Introduction

Many experiments relevant to today's research use lasers to identify atomic and molecular species, from both fundamental and applied viewpoints. Some of the natural processes under investigation, however, occur in challenging environments or in places with limited optical access. Examples of such experiments include measurements of reactive flows, remote natural settings, or emissions of hazardous gases [1], [2]. The most widely used laser diagnostics methods for the examples given are Raman scattering and laser-induced fluorescence (LIF). These are both incoherent emissions that emit approximately isotropically, thus providing very low-intensity signals [3]. Since these methods yield incoherent light whose intensity decreases quadratically with distance, remote sensing with them becomes extremely challenging [1].

Directed emission, preferably in the form of a coherent beam, would result in a significantly more localised signal, compared to the ones described above. One such type of emission is mirrorless lasing [2], [1]. This emission is generated by focusing a pump laser beam into a collection of atoms or molecules, thereby creating a population inversion that, in turn, leads to collective light emission [4], [1]. The gain medium will be defined by the region experiencing the highest intensity, since the population inversion is strongest there [5]. This emission is thus cavity-free, further promoting its advantage for challenging measurement conditions. An illustration of how mirrorless lasing can be achieved is shown in Figure 1.

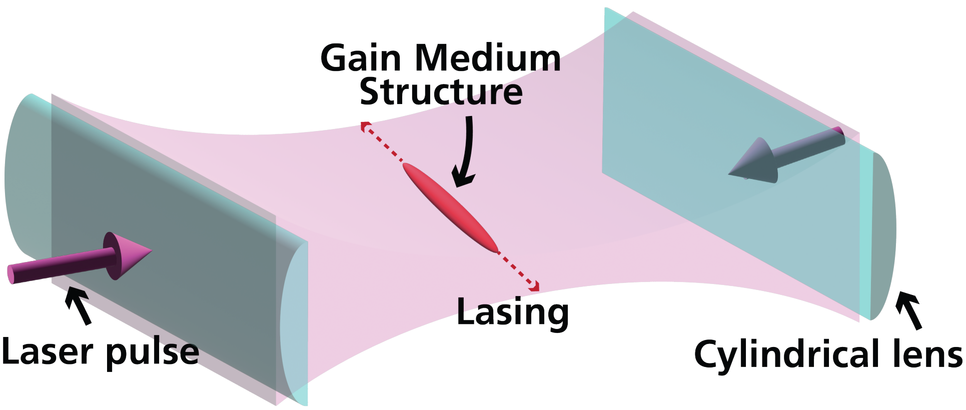

Figure 1: An illustration of mirrorless lasing and the construction of the gain medium.

The direction of emission will be along the longest path of the gain medium [5]. This is due to the generated emission being able to interact with the largest number of excited atoms along this path. The conclusion implies that the direction of emission is fully determined by the gain medium's orientation, which in turn is set by the pump beam's focus geometry. As shown in Figure 1, a cylindrical lens will generate emission perpendicularly to the pump laser beam, both in the forward and backward direction. On the other hand, a spherical lens will generate emission along the pump beam direction. Such a property suggests that it is possible to control the emission direction in mirrorless lasing by solely changing the pump laser's focus. This allows for great versatility, which is highly advantageous in challenging measurement conditions where, e.g., optical access is limited. Furthermore, well-known, coherent techniques such as coherent anti-Stokes Raman spectroscopy (CARS) and stimulated Raman scattering lack this property [2].

These emit radiation in a fixed direction strictly determined by conservation of momentum. Mirrorless lasing thus presents itself as a highly promising and more adaptable laser diagnostics method.

In order to fully utilise the versatility of mirrorless lasing, it is necessary to thoroughly investigate how the emission behaves as a function of the gain medium geometry. However, very little research has previously been made on this subject. To the author's knowledge, there are only two publications: the first made by Dogariu and Miles (2020), and the second by Dominguez et al. (2025). These research articles discuss the possibility of mirrorless lasing emission perpendicularly to the pump beam direction, a phenomenon known as sideways lasing. It would thus be of interest to further investigate how the mirrorless lasing direction can be modified through gain medium alterations, and how such changes of the gain medium geometry would affect the emission.

It is, however, not only direction modifications of mirrorless lasing that lack thorough investigation, but also the light-matter interaction occurring during the emission process. Without this knowledge, the implementation of mirrorless lasing as a laser diagnostic method is unachievable, since the species information is highly dependent on the type of interaction. Different sources state various explanations, suggesting that more information on the subject is needed [6], [5].

This thesis seeks to fundamentally investigate mirrorless lasing in atmospheric pressure environments, with the goal of acquiring information vital for future applications. The two main research subjects are (1) how the mirrorless lasing depends on the gain medium structure and (2) what light-matter interaction is responsible for the emission. To investigate the first of these two, a gain medium with theoretically known emission behaviour was chosen. This way, the subsequent analysis would be greatly facilitated. Furthermore, a gain medium generating sideways lasing was chosen in order to avoid having to filter out the pump beam. By conducting both temporal and spatial measurements of the emitted mirrorless lasing, substantial information about the atomic process causing the emission can be obtained.

1.1 Outline of the Thesis

The thesis starts by presenting existing theory relevant to the project. Section **2.1** outlines all atomic and quantum physics necessary to explain the experiments and observed results. This includes all relevant atomic emission processes, such as stimulated emission, spontaneous emission, amplified spontaneous emission (ASE), and superfluorescence (SF), as well as the quantum-mechanical descriptions necessary to fully describe them. Following this, Section **2.2** presents the two laser diagnostic methods involved in this project: two-photon laser-induced fluorescence (TALIF) and mirrorless lasing. To the best of the author's knowledge, there exists no other body of text explaining the connection between different atomic emission processes and experimentally generated mirrorless lasing to this extent. Furthermore, Section **2.3** includes a description of the physical processes involved in streak camera imaging.

Following the theory, Section **3** describes the experimental method of the project. The experimental setup used is illustrated and described in Section **3.1**, while Sections **3.2** and **3.3** describe the spatial and temporal measurements of mirrorless lasing, respectively.

The results and discussion of the experiments are both included in Section **4**. The structure of this section mimics that of Section 3 in order to facilitate the reading experience.

Finally, Section **5** presents the project's conclusions, while Section **6** provides an outlook, describing possible future experiments based on the discoveries made in this project.

2 Theory

2.1 Light-Matter Interaction Processes

Light can be seen as electromagnetic radiation, thus including an oscillating electric field [7]. Considering a two-level atom interacting with such an oscillating field, the time-dependent Schrödinger equation (TDSE) contains a Hamiltonian consisting of two parts,

$$i\hbar\frac{\partial\Psi}{\partial t} = \hat{H}\Psi,\ \hat{H} = \hat{H}_0 + \hat{H}_I(t)\ .$$

Here $\hat{H}_I(t)$ gives the interaction with the electric field as a perturbation, and $\hat{H}_0$ describes an unperturbed system and the atomic energy levels in it. Assuming the radiation from the oscillating field has a wavelength much longer than the size of the atom, one can use the dipole approximation to describe $\hat{H}_I(t)$. It is then given by,

$$\hat{H}_I(t) = e\mathbf{r}\cdot\mathbf{E}_0\mathrm{cos}(\omega t)\ ,$$

where $-e\mathbf{r}$ is the electric dipole induced by the electric field, $\mathbf{r}$ is the position of the electron relative to the atom's centre of mass, $\mathbf{E}_0$ is the amplitude of the field, and ω is the angular frequency of it [7]. Furthermore, one can make the ansatz that the wavefunction of the atom at all times can be described by the following superposition of the two energy states $|1\rangle$ and $|2\rangle$,

$$\Psi(\mathbf{r},t) = c_1(t)\,|1\rangle\,e^{-i\omega_1 t} + c_2(t)\,|2\rangle\,e^{-i\omega_2 t}\ .$$

Here, ω_1 and ω_2 are the frequencies of the lower and upper atomic energy states, respectively. Normalization also requires that $|c_1|^2 + |c_2|^2 = 1$.

Solving the TDSE for the expression of $\Psi(\mathbf{r},t)$ stated above, yields the two following differential equations,

$$i\dot{c}_1 = \Omega\mathrm{cos}(\omega t)e^{-i\omega_0 t}c_2 \tag{1}$$
$$i\dot{c}_2 = \Omega^*\mathrm{cos}(\omega t)e^{i\omega_0 t}c_1 \tag{2}$$

where $\omega_0 = \omega_2 - \omega_1$ is the frequency difference between the two states. Ω is the Rabi frequency, given by

$$\Omega = \frac{\langle 1|\,e\mathbf{r}\cdot\mathbf{E}_0\,|2\rangle}{\hbar} = \frac{e\,\langle 1|\,u\,|2\rangle\,|E_0|}{\hbar} = \frac{eU_{12}|\mathbf{E}_0|}{\hbar}\ ,$$

for interactions with a unidirectional field that is linearly polarised along an arbitrary axis, here denoted as u. Solving Equations (1) and (2), using time-dependent perturbation theory and the weak-field approximation, which assumes that the probability amplitude of the atom being in state $|1\rangle$ remains roughly equal to one over time, i.e. $c_1(0) = 1$, $c_2(0) = 0$, and $c_1(t) \approx 1$, one obtains

$$|c_2(t)|^2 = \left|\Omega \frac{\sin[(\omega_0 - \omega)t/2]}{\omega_0 - \omega}\right|^2 \ ,$$

where $|c_2(t)|^2$ is the population of state $|2\rangle$. Taking the integral of this expression, for the case of broadband, unidirectional, and linearly polarised radiation along an arbitrary axis u over a frequency interval, the following expression for the transition rate between state $|1\rangle$ and $|2\rangle$ is derived,

$$R_{12} = \frac{|c_2(t)|^2}{t} = \frac{\pi e^2 |U_{12}|^2}{\epsilon_0 \hbar^2} \rho(\omega_0) \tag{3}$$

where $\rho(\omega_0)$ is the energy density in the frequency interval ω_0 to $\omega_0 + \mathrm{d}\omega$. A more detailed derivation of Equation (3) is found in literature by Foot (2005, p. 126). It has to be noted that this derivation is made specifically for light polarised along the x-axis.

Stimulated Absorption and Emission

The process of stimulated absorption is defined as the atom's absorption of a photon, following its interaction with an external radiative field [7]. It is characterized by the Einstein coefficient B_{12}, which is the proportionality constant of the absorption rate $R_{12} = B_{12}\rho(\omega_0)$. This implies that B_{12} can be derived from the solution of the TDSE for $|1\rangle$ and $|2\rangle$. Thus, using Equation (3) one obtains

$$B_{12} = \frac{\pi e^2 |U_{12}|^2}{\epsilon_0 \hbar^2} \ .$$

Due to symmetry, the probability of transitions from the upper state $|2\rangle$ to the lower $|1\rangle$ should be equal to the probability of absorption. This process, known as stimulated emission, results in the emission of a photon with the same properties as the photon of the interacting radiative field. The transition is characterised by the Einstein coefficient B_{21}. Because of symmetry, $B_{12} = B_{21}$.

The intensity of a beam, being amplified through stimulated emission, and emitted from a single pass through a medium with length L, is

$$I(L) = I(0)e^{\gamma(\nu)L} \ , \tag{4}$$

where $\gamma(\nu) = \Delta N \sigma(\nu)$ is the gain coefficient [8]. $\Delta N = N_2 - N_1$ is the difference between the population densities N_1 and N_2 in the energy states $|1\rangle$ and $|2\rangle$ respectively. $\sigma(\nu)$ is the transition cross section at frequency ν. This suggests that stimulated emission will display a threshold behaviour, since ΔN needs to be positive in order for the gain to be positive.

Spontaneous Emission

Spontaneous emission is the emission of a photon following the transition of the atom from $|2\rangle$ to $|1\rangle$, when no external radiative field is present. The photon is then emitted due to vacuum-field fluctuations [9]. These are fluctuations that are present as a result of the system's energy at zero temperature being non-zero. Thus, even at the lowest possible energy, the electric field still has a certain magnitude. This effect results in the generation of a stronger electric field, known as the radiation reaction field, which causes a minimal dipole moment. The radiation reaction field will interact with the atom, successively driving its population down from the upper to the lower energy state. This field will thus transport energy out of the atom, thereby causing a photon to be emitted and completing the spontaneous emission. The phases of the emitted photons will be random, which implies that they are not expected to interfere [10]. Due to the photons also being emitted in random directions and with random polarisation, spontaneous emission lacks spatial and temporal coherence, directionality, and a fixed polarisation.

The process of spontaneous emission is characterised by the Einstein coefficient A_{21} [7]. It is related to B_{21} by

$$A_{21} = \frac{\hbar\omega^3}{\pi^2 c^3} B_{21} \ .$$

The mean lifetime of the upper state $|2\rangle$, given by T_1, is also connected to A_{21} in the following way,

$$A_{21} = \frac{1}{T_1} \ .$$

The time duration of the spontaneous emission is thus T_1. Furthermore, the lifetime given by T_1 is only connected to the populations of the upper and lower energy states. For most atoms and molecules, this lifetime is on the order of nanoseconds [11]. The intensity of spontaneously emitted photons from a collection of atoms with a length L, follows the relation

$$I(L) = C N_2 A_{21} h\nu L,$$

where $h\nu$ is the energy of one photon with frequency ν, and C is a geometrical constant, which is dependent on the detection geometry [12]. The expression above implies that spontaneous emission lacks an intensity threshold.

Rabi Oscillations

It is possible to solve Equations (1) and (2), for an external field that is not weak; i.e. without the constraint $c_1(t) \approx 1$ [7]. Rewriting the two differential equations to

$$\begin{aligned} i\dot{c}_1 &= \frac{\Omega}{2}\left[e^{i(\omega-\omega_0)t} + e^{-i(\omega+\omega_0)t}\right] c_2 \\ i\dot{c}_2 &= \frac{\Omega^*}{2}\left[e^{i(\omega+\omega_0)t} + e^{-i(\omega-\omega_0)t}\right] c_1 \ , \end{aligned}$$

and using the rotating-wave approximation to eliminate the fast oscillating $(\omega + \omega_0)t$-terms, one obtains

$$
\begin{aligned}
i\dot{c}_1 &= \frac{\Omega}{2} e^{i(\omega - \omega_0)t} c_2 \\
i\dot{c}_2 &= \frac{\Omega^*}{2} e^{-i(\omega - \omega_0)t} c_1 \ .
\end{aligned}
$$

These equations can be rewritten to

$$
\frac{\mathrm{d}^2 c_2}{\mathrm{d}t^2} + i(\omega - \omega_0)\frac{\mathrm{d}c_2}{\mathrm{d}t} + \left|\frac{\Omega}{2}\right|^2 c_2 = 0 \ ,
$$

which at resonance ($\omega_0 = \omega$) has the solution

$$
|c_2(t)|^2 = \sin^2\left(\frac{\Omega t}{2}\right) \ .
$$

The above expression suggests that the population of the upper state $|2\rangle$ and lower state $|1\rangle$ oscillates with a frequency equal to the Rabi frequency Ω at the resonance wavelength. These oscillations are therefore known as Rabi oscillations.

The Bloch Sphere

In order to conveniently describe the quantum state of an atom and how it is affected by an external radiative field, one can use the density matrix, defined as follows,

$$
|\Psi\rangle \langle\Psi| = \begin{pmatrix} |c_1|^2 & c_1 c_2^* \\ c_2 c_1^* & |c_2|^2 \end{pmatrix} = \begin{pmatrix} \rho_{11} & \rho_{12} \\ \rho_{21} & \rho_{22} \end{pmatrix} \ [7].
$$

The diagonal terms are, as already stated, the populations of the states $|1\rangle$ and $|2\rangle$. The off-diagonal terms are the coherences. These define the induced dipole moment, and thus describe how the atom responds to the external field. ρ_{12} corresponds to the transition between state $|1\rangle$ and $|2\rangle$, while ρ_{21} corresponds to the transition between state $|2\rangle$ and $|1\rangle$.

By defining new variables $\tilde{\rho}_{12} = \rho_{12}e^{-i\delta t}$, $\tilde{\rho}_{21} = \rho_{21}e^{i\delta t}$, where $\delta = \omega - \omega_0$ is the detuning from the resonance angular frequency ω_0, one obtains the following set of equations,

$$
\begin{aligned}
u &= \tilde{\rho}_{12} + \tilde{\rho}_{21} \\
v &= -i(\tilde{\rho}_{12} - \tilde{\rho}_{21}) \\
w &= \rho_{11} - \rho_{22} \ .
\end{aligned}
$$

The new variables include the response of the system when it interacts with radiation that is not at the resonance frequency. This set of equations can then be used to define the Bloch vector $\mathbf{R} = u\hat{\mathbf{e}}_1 + v\hat{\mathbf{e}}_2 + w\hat{\mathbf{e}}_3$. The Bloch vector has a magnitude equal to unity and maps out the surface of the so-called Bloch sphere. This sphere includes all the information necessary to describe the state in which a two-level atomic system can exist. A schematic illustration of the Bloch sphere is shown in Figure 2 below.

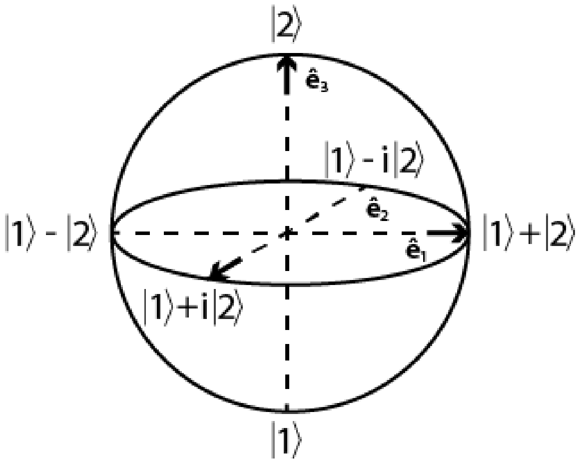

Figure 2: The Bloch sphere including the unit vectors and a few surface states.

The positions of the two poles of the sphere correspond to the atom being in either the $|1\rangle$ or $|2\rangle$ state. All other locations on the sphere correspond to a superposition state. For an atom existing in a resonant external field, the Bloch vector will rotate in the sphere with a frequency equal to Ω. States on the surface of the sphere correspond to states with the maximum amount of known information [13]. These are known as pure states. The states confined within the sphere are known as mixed states.

Since the coherence, and thus the induced dipole moment, is given by the off-diagonal terms in the density matrix, it is determined by the superposition of the two states. In the Bloch sphere, the superposition states are defined by the $\hat{\mathbf{e}}_1\hat{\mathbf{e}}_2$-plane. Therefore, the projection of the vector for the state in question on the $\hat{\mathbf{e}}_1\hat{\mathbf{e}}_2$-plane yields the degree of coherence. A vector with length zero residing at the centre of the sphere corresponds to the state with complete incoherence. This reasoning also implies that the coherence of atoms located in state $|1\rangle$ or $|2\rangle$ is zero.

An important physical property dictating the temporal evolution of an atomic state is the average transition time from state $|2\rangle$ to $|1\rangle$, or lifetime, T_1 [14]. Another important property is the coherence time, T_2. This is the time required for the superposition state to lose its coherence. In general it holds that $T_2 \leq 2T_1$.

Coherence Properties of Stimulated and Spontaneous Emission

Stimulated emission occurs as a response of the atomic system to an external radiative field [9]. The external field will, as stated, induce a dipole moment in the atom, which will result in the deviation from the upper state $|2\rangle$. The dipole will oscillate at the frequency of the external field, since that is what induces it. Because the field generated by the dipole moment has a phase and frequency set by the external field, no information is lost, ensuring that the emission from this process is fully coherent. Using the Bloch sphere formalism, the atom can be seen as travelling along the surface of the sphere, towards the lower state $|1\rangle$ [7]. The atom thus enters a superposition state which has an energy lower than the upper state $|2\rangle$. In order for the energy in the system to be conserved during this transition, the atom therefore needs to have emitted energy. Upon reaching the lower state $|1\rangle$, the decrease in energy of the system corresponds to the energy difference between $|2\rangle$ and $|1\rangle$. This energy has then been transported out of the system in the form of a single photon with the same frequency and phase as the external radiative field.

In contrast to the case of stimulated emission, the process of spontaneous emission does not involve a radiative field [9]. As previously stated, the emission process occurs as a result of vacuum-field fluctuations inducing a radiation reaction field. Since the vacuum-field fluctuations have both random phases, polarisations, and directions, it is impossible to know about any of these properties of the field inducing the spontaneous emission. Therefore, the emitted photon lacks both spatial and temporal coherence. Since $T_2 \leq 2T_1$ holds in general, the reasoning above is consistent with the stated theory. In the Bloch sphere, spontaneous emission thus corresponds to a shrinking of the Bloch vector towards the middle of the sphere, ending up in $|1\rangle$.

Time Duration of Stimulated Emission

As previously stated, the process of stimulated emission corresponds to the Bloch vector tracing a path along the surface of the sphere from $|2\rangle$ to $|1\rangle$ [7]. This path corresponds to the vector moving with an angle π. Since the vector moves with frequency Ω in a resonant external field, the time duration of the stimulated emission is,

$$t_\pi = \frac{\pi}{\Omega} \, , \tag{5}$$

assuming that the Rabi frequency Ω has the unit rad/s. For strong external fields given by ultrafast lasers, one can obtain Rabi frequencies in the THz range, yielding values of t_π around tens of femtoseconds [15].

2.1.1 Amplified Spontaneous Emission (ASE)

The process of amplified spontaneous emission, or ASE, is defined as the amplification of spontaneously emitted photons [16]. ASE is initiated by a few photons spontaneously emitted in a gain medium with population inversion. These photons will then induce stimulated emission in the still excited atoms, thereby amplifying the initially emitted photons.

Population inversion, which is required for obtaining ASE, can be defined as when $\Delta N = N_2 - N_1 > 0$ [8]. It also holds that $E_{|2\rangle} > E_{|1\rangle}$. This definition thus implies that the higher energy level has to have a higher population density than the lower in order for the system to have population inversion. It is necessary for this condition to be fulfilled in a laser if any amplification of an incoming photon is to be achieved.

Since ASE is initiated by several spontaneously emitted photons, all having random phases and directions, it lacks temporal coherence despite the signal being amplified through stimulated emission [16]. This separates ASE from the coherent emission generated by a laser. In a laser, the presence of a cavity selects a certain spatial mode, which then dictates the phase and polarisation [8]. This ensures that laser emission has a higher optical output power and narrower linewidth FWHM compared to ASE [16]. When using a mode-locked laser, ASE is commonly seen as noise, causing fluctuations in pulse energy and phase [17]. It is therefore seen as an unwanted type of emission in that context.

For the variation in intensity of ASE at frequency ν and along an axis z, it follows that

$$\frac{\partial I_\nu}{\partial z} = \sigma \Delta N I_\nu + C N_2 A_\nu h\nu \ , \tag{6}$$

where σ is the cross section of the transition, A_ν is the spectral rate of spontaneous emission, and C is a geometrical constant [12]. For the case of a strong external field, yielding a large value of ΔN, I_ν grows exponentially with ΔN. However, for the case of a small value of ΔN, I_ν will be weak, resulting in only the second term of Equation (6) surviving. The intensity of the ASE will then be linearly dependent on N_2. These relations suggest that ASE will display a threshold behaviour; for an external field strong enough, the ASE intensity will increase drastically.

Due to its physical properties, the time duration of an ASE emission depends on three factors. The first is the time duration of the spontaneous emission, determined by T_1, which initiates the process. The second is the time duration of the stimulated emission, which is governed by Equation (5). Furthermore, the time it takes for the photons to propagate through the gain medium, given by

$$t_p = L/c \ , \tag{7}$$

also has an essential role in determining the time duration of the ASE [18]. It can be noted that t_p determines the shortest pulse duration possible for ASE, since the emission is built up through propagation. If L is on the order of 1 cm and the emission is travelling through air, $t_p \approx 30$ ps.

2.1.2 Superfluorescence (SF)

Superfluorescence (SF) is a cooperative emission process [18]. It is a special case of the emission process superradiance, where macroscopically coherent atomic dipoles couple together through a common external field [19]. SF distinguishes itself by involving macroscopically incoherent atomic dipoles, which spontaneously develop macroscopic coherence through vacuum-field fluctuations. This process implies that the radiation emitted through SF is both spatially and temporally coherent.

In order to achieve this type of emission, it is necessary to have a gain medium with population inversion [18]. This can be achieved with an external pump laser. To explain the emission process, it is useful to utilise the Bloch sphere formalism. Defining the sum of all individual Bloch vectors as a macroscopic Bloch vector, it is possible to monitor changes in the system of atoms through the position of the vector in the corresponding macroscopic Bloch sphere. The process of SF starts with a few of the atoms in the medium spontaneously emitting photons due to the presence of vacuum-field fluctuations. Summing up the individual Bloch vectors for each atom, the macroscopic Bloch vector has been tipped with a small angle θ^i [18]. Now, the macroscopic Bloch vector has a non-zero projection onto the $\hat{\mathbf{e}}_1\hat{\mathbf{e}}_2$-plane, meaning that the whole system can be considered to have a minuscule dipole moment.

As the spontaneously emitted photons interact with the excited atoms, the radiation from them induces dipole moments in other atoms [18]. There is then a larger number of atoms in the gain medium that will have entered a superposition state, thus pushing the macroscopic Bloch vector further down the Bloch sphere. This leads to an increased coherence and dipole moment of the entire system, causing the system to oscillate in phase more and more. The change of the angle θ over time relates to θ in the following way

$$\frac{\mathrm{d}\theta}{\mathrm{d}t} = \frac{1}{2T_R}\sin(\theta)\ . \tag{8}$$

T_R is defined as the superradiance time, describing the lifetime of the collective state. It is given by

$$T_R = \frac{T_1}{\mu N}\ , \tag{9}$$

where μ is a geometrical factor, proportional to the diffraction solid angle of the gain medium, and N is the number of atoms contributing to the generated field, which initially is equal to the number of excited atoms. This suggests that the lifetime of the collective state decreases for a higher value of N. Equation (8) thus describes the oscillation of the macroscopic Bloch vector, which corresponds to a radiative field.

For smaller values of θ, such as in the initial state, Equation (8) can be solved using the small-angle approximation. The angle θ then grows exponentially over time. As θ becomes larger, this approximation stops holding, leading to a slower increase in it. At $\theta = \pi/2$, $\sin(\theta) = 1$, meaning that the induced dipole moment in the collective state has reached its maximum value. After having reached the maximum value, the number of atoms in the excited state has decreased significantly. This leads to the macroscopic Bloch vector continuing to move down along the Bloch sphere. Therefore, the projection of the Bloch vector decreases, leading to a decreased radiative field. The rate that the Bloch vector moves ($\frac{\mathrm{d}\theta}{\mathrm{d}t}$) corresponds to the Rabi frequency; however, in this case, no external radiation is present. The Rabi frequency, thus, is in this case self-induced, since it depends on θ, which grows due to the internal radiative field.

Using Equation (8) together with Bloch equations and an initial value θ^i, yields the following expression for the intensity of the emitted SF pulse,

$$I(t) = \frac{\hbar\omega_0 N}{2T_R}\mathrm{sech}^2\left[\frac{(t - t_D(\theta^i)}{2T_R}\right]\ , \tag{10}$$

where t_D is the delay time between the excitation pulse generating the population inversion, and the peak of the SF emission. SF will display a threshold behaviour in the emitted intensity since the process cannot be achieved if the coherence time T_2 is too short in comparison to T_R, which depends on the value of N [20]. In Equation (10), t_D is written as a function of θ^i and can be expressed as

$$t_D(\theta^i) = -2T_R \log\left(\frac{\theta^i}{2}\right) \ . \tag{11}$$

It can be noted that t_D decreases with an increasing value of N. This is due to T_R being inversely proportional to the quantity, according to Equation (9). The delay time t_D also depends on the magnitude of the initial angle; a small value of θ^i yields a long t_D, while a large value yields a short t_D. Previous measurements of t_D gave values with the magnitude of tens of picoseconds for atoms and molecules in gaseous form [21], [22].

Now assume that one has a gain medium where the length L of it obeys $L \gg \lambda$, where λ is the emission wavelength [18]. This implies that the atoms are not located at a point, but rather confined to a longer medium. Such a configuration is significantly easier to achieve experimentally. For such a gain medium, the photons spontaneously emitted in the direction with the largest number of excited atoms will exist longer in the system. These photons are thus able to induce dipole moments in a larger number of excited atoms, thereby dictating the phase of more atoms. This implies that the final collective phase the system attains is governed by the phase of the initial spontaneous emissions seeding the process, as well as by the phase of the photons travelling in directions that yield the highest gain.

If the gain medium has a cylindrical shape that fulfils $L \gg w$, where $2w$ is the transverse width of the medium, it has a so-called pencil shape [18]. In that case, it also holds that the Fresnel number $F = \pi w^2/L\lambda \ll 1$. The geometrical angle $\theta_G = \tan^{-1}(w/L)$ will then be smaller than the diffraction angle $\theta_D = \sin^{-1}(\lambda/w)$, suggesting that only one transversal mode can survive. The relatively large diffraction angle will also provide a Fraunhofer diffraction pattern [18], [8]. There will, however, be additional intensity variations transversely across the beam. Since most radiation sources yielding the needed population inversion of the system have a Gaussian intensity profile, the gain medium will have an uneven distribution of excited atoms, yielding an uneven refractive index [23]. As collective dipole moments are built up at different locations along the width of the gain medium and then interfere, an interference pattern is generated. For geometries with $F \ll 1$, this is an important effect. If the gain medium has a cylindrical shape, the generated interference pattern will consist of circular shapes, due to the pattern in the far field being a Fourier transform of the source shape [8].

The atoms with induced dipole moments carry intrinsic phases, given by the radiative field interacting with them [18]. When observing the emission along a given direction $\mathbf{k}_0$, one obtains a phase shift connected to that specific direction. This is due to atoms in different locations along the gain medium having to travel different lengths before they are detected, thus acquiring different phase shifts. The atoms radiating in the direction $\mathbf{k}_0$ will then have phase shifts exactly cancelling the phase shifts induced by the observation. That is, an atom interacting with the radiative field in direction $\mathbf{k}_0$ earlier will also have to travel a longer distance before being detected, thus cancelling the phases. This is the case for all atoms radiating along $\mathbf{k}_0$, leading to the intensity of the emitted signal being proportional to N^2.

For a longer gain medium, so-called superradiance ringing will appear over time. This ringing is an effect of different regions in the medium experiencing radiative fields of different strengths. The atoms located at the end of the gain medium will experience a stronger radiative field, compared to the atoms located at the beginning of the medium, due to interaction with a larger number of emitted photons. When the atoms at position L have individual Bloch vectors with $\theta = \pi$, their individual dipole moments are equal to zero. However, atoms located at positions before L have not yet had time to reach state $|1\rangle$, implying that their individual Bloch vectors still have an angle $\theta < \pi$. The atoms at L can reabsorb this radiative field and are therefore driven up the Bloch sphere, leading to the macroscopic Bloch vector "overshooting" $\theta = \pi$. The generated field will, however, be phase-shifted by π, leading to this field cancelling out the previously generated field. One can observe this cancellation as a drop to zero intensity. As the atoms, having reabsorbed radiation, react with the other atoms in the medium, they once again emit photons, creating a second emission peak. This can occur several times, resulting in the behaviour shown in Figure 3.

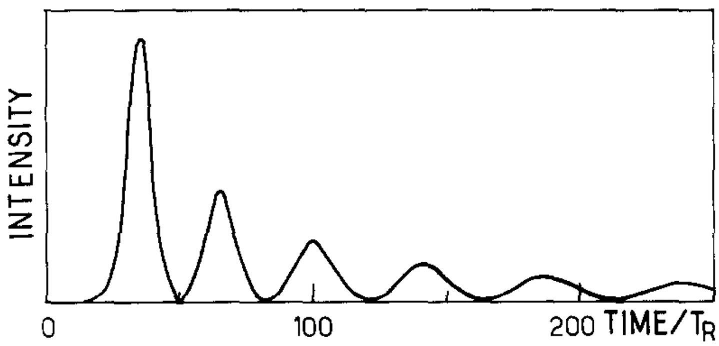

Figure 3: Theoretical prediction of superradiance ringing for a system where $F = \pi w^2/L\lambda \ll 1$ [18].

Since the radiative field that the atoms at L can reabsorb is weaker than the original field that they absorbed, the second emission peak has a lower intensity than the first. This is due to photons also being able to escape the gain medium when they have reached L, leading to the created radiative field steadily decreasing. It can be observed that the oscillatory behaviour does not have a constant frequency. This is due to the movement of the Bloch vector in time, and thus the emission envelope, being governed by the internal Rabi frequency $\frac{\mathrm{d}\theta}{\mathrm{d}t}$. As the radiative field decreases, so does the maximum angle θ with which the Bloch vector can be tilted from $\theta = \pi$. According to Equation (8), the internal Rabi frequency will decrease as θ approaches π. Therefore, the frequency of the oscillations will decrease over time, something that is clearly visible in Figure 3. The contrast of the ringing increases for smaller θ^i. This suggests that a longer delay time leads to a more pronounced collective behaviour, resulting in a higher degree of coherence.

More recent research suggests that one also has to account for propagation effects created by the induced dipole moments [24]. Such effects become important for high values of N. It is then suggested that when N is essentially constant, the intensity of the emitted SF pulse is best described using Bessel functions, rather than the expression given in Equation (10). The use of such functions instead would imply that oscillations should be observed also during the incline of the SF pulse.

2.1.3 Comparison of the Presented Emission Processes

In order to facilitate the comparison of the different emission processes presented in this section, Table 1 displays the most important physical properties of these emission types.

Emission type	**Coherent**	**Time Duration**	**Threshold**	**Intensity Profile**
Stimulated Emission	Yes	fs	Yes	Exponential
Spontaneous Emission	No	ns	No	Linear
ASE	No	ps	Yes	Exponential
SF	Yes	ps	Yes	Quadratic

Table 1: A table comparing the four emission processes presented in this section. Note that all of the time durations are set at the order of magnitude relevant for this thesis and that these can change significantly for other experimental conditions. It is also important to note that the intensity of ASE only grows exponentially for high pump laser intensities. The intensity profile here refers to the dependence of emission intensity on either ΔN, N_2, or N, depending on the emission type.

It is important to be aware that for a process to be characterised as coherent in the table above, it needs to be both spatially and temporally coherent.

2.2 Laser Diagnostics

Laser diagnostics are measurement techniques involving lasers that allow for non-intrusive, in-situ, remote, and temporally and spatially precise measurements [3]. Such techniques make it possible to perform high-accuracy measurements on many challenging processes, such as ultrafast events and highly susceptible objects. Two commonly used laser diagnostic techniques presented in this section are laser-induced fluorescence (LIF) and two-photon absorption laser-induced fluorescence (TALIF). Furthermore, a less well-known technique, mirrorless lasing, will also be described.

2.2.1 Laser-Induced Fluorescence (LIF)

Fluorescence is the process of spontaneous emission following the excitation of an atom or molecule [3]. The excitation from a lower state E_1 to a higher state E_2 can be achieved through the absorption of one or more photons. If, upon relaxation, the particle returns to the same lower state as the initial one (here E_1), the process is known as resonant fluorescence. When the excitation is achieved with a laser, the process is called laser-induced fluorescence or LIF. Figure 4 illustrates the process of single-photon LIF.

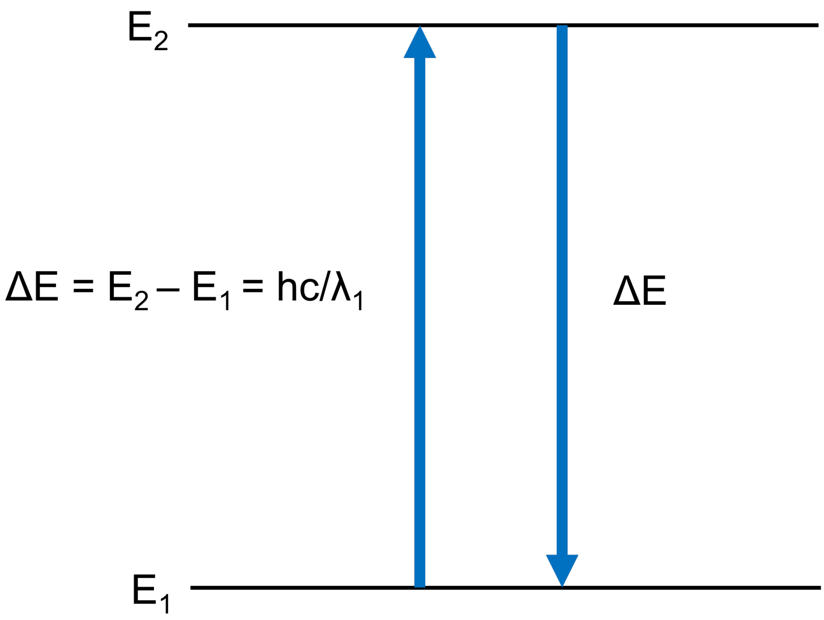

Figure 4: A diagram depicting the process of one-photon resonant LIF. λ_1 corresponds to the wavelength of the incoming laser, which is the wavelength needed to drive the transition.

The transition probability of LIF is proportional to the intensity I of the incoming laser beam, making it a linear process [25]. The cross-section of a LIF event is on the order of 10^{-16} cm^2 [26].

2.2.2 Two-photon Absorption Laser-Induced Fluorescence (TALIF)

As stated, it is possible to obtain fluorescence, and thereby also LIF, through the absorption of more than one photon. This is known as two-photon absorption laser-induced fluorescence, or TALIF. For the case of two-photon absorption, the sum of the photon energies will equal the energy needed to reach the excited state [27]. The transition will go through a virtual intermediate state E_i. A diagram of the absorption process is shown in Figure 5.

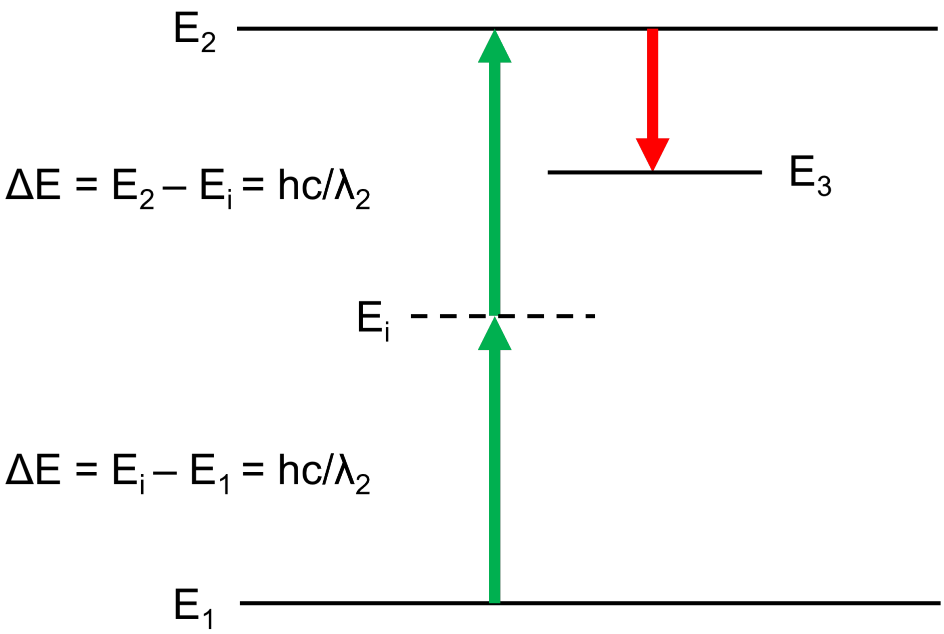

Figure 5: A diagram depicting the process of TALIF, where the absorbed photons have equal energy. λ_2 corresponds to the wavelength of the incoming laser. This is twice as long as the wavelength needed to drive the transition, i.e. $\lambda_2 = 2\lambda_1$. Note that the atom does not return to the initial state through the process of single-photon emission. This is due to single-photon transitions being forbidden, where two-photon transitions are allowed [28].

In order for the excitation to be possible, the two photons have to arrive within the lifetime of the intermediate state, which is less than 1 fs [25]. The lifetime is determined by the Heisenberg uncertainty principle, stating that $\Delta\tau \leq \hbar \cdot \delta E$, where δE is the energy difference between the E_1 state and the closest real energy state. In contrast to LIF, TALIF is a nonlinear process with a transition probability scaling with I_p^2 for a single laser beam, where I_p is the intensity of the pump laser [29]. Thus, for two-photon absorption, it holds that $N_{ex} \propto I^2$, where N_{ex} is the number of excited atoms [30]. The cross section of TALIF is also significantly lower, being on the order of 10^{-50} cm$^4\cdot$ s. Despite the lower cross section, TALIF is an important method for exciting transitions which have energy differences corresponding to wavelengths in the vacuum ultraviolet (VUV) regime [31]. Since the wavelength for each individual photon can be twice as long for TALIF, it is possible to probe such transitions in air using this process, thereby greatly facilitating many spectroscopic experiments. Furthermore, due to transitions allowing two-photon excitation being forbidden for single-photon excitation, TALIF is also a useful complementary method to LIF [28].

2.2.3 Mirrorless Lasing

A laser is required to contain three components: a pumping mechanism, a gain medium, and a feedback loop [4]. The latter usually consists of two reflective surfaces, such as mirrors [8]. Mirrorless lasing is defined as the generation of directed light without a feedback loop generated by external components [4]. There can, in certain cases, still exist weaker feedback, from processes such as multiple scattering, but in general, mirrorless lasing can be considered to be single-pass emission due to the lack of reflective components [4], [32]. This emission can be generated using quantities of several different atoms or molecules as the gain medium; however, if it is generated with air as the gain medium, it is known as air lasing. The gain medium can then consist of any of the atomic or molecular species present in air [32]. Due to the emission being generated by a single pass through the gain medium, it is necessary to choose a species that generates strong optical gain in order to obtain a strong emission. Depending on the atom or molecule used, the emission will be different, thereby yielding species information. For both mirrorless lasing and actual lasers, the pumping mechanism is used to create population inversion in the gain medium [4].

As previously stated in Section 2.1, the probability of stimulated emission and stimulated absorption is equal. This, in turn, implies that population inversion is impossible to obtain in a two-level energy system. Therefore, it is necessary to use either a three-level or four-level energy system to achieve population inversion. It is then possible to effectively pump up to the highest state, which then generates population in the state below it by spontaneously decaying to it. The population inversion will then be obtained between the first excited and ground state in a three-level system, or between the second and first excited state in a four-level system. Figure 6a) and b) shows illustrations of a three- and four-level system, respectively.

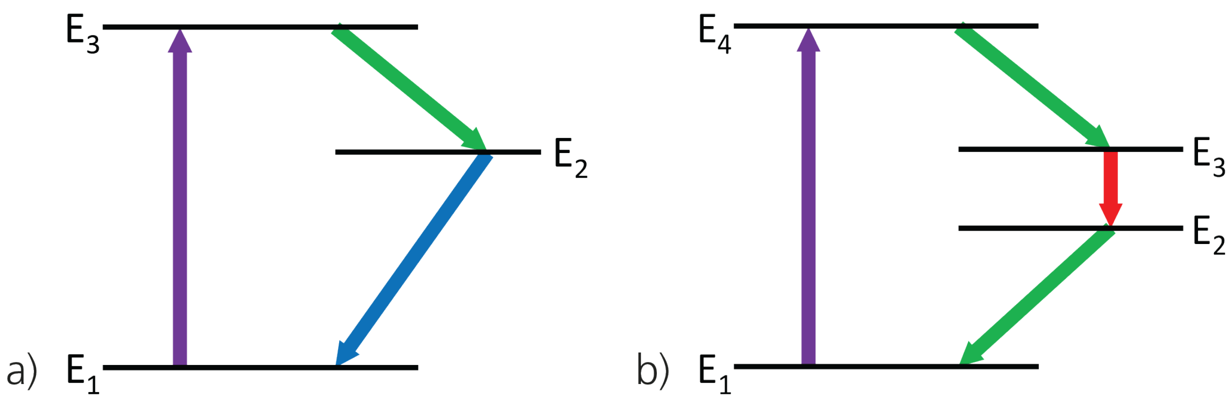

Figure 6: Illustrations of three- and four-level atomic systems. a) An example of a three-level system. b) An example of a four-level system.

Since there is no cavity restricting the path of the generated emission in mirrorless lasing, the direction of the emission is fully determined by the geometry of the gain medium [5]. The emission direction will be along the longest path in the gain medium. This is because the emission occurs after a single pass in the gain medium, and a longer path will result in the interaction with a larger number of excited atoms, and thus a stronger signal. When performing air lasing, or mirrorless lasing in a gas, the gain medium is pumped by directing a focused laser beam into the gas. The gain medium will then be located in the region around the focus of the pump beam. This is due to the intensity of the pump beam, and thus also the gain, being the highest there.

As is illustrated in Figure 7, the usage of different focusing lenses will create different gain medium structures.

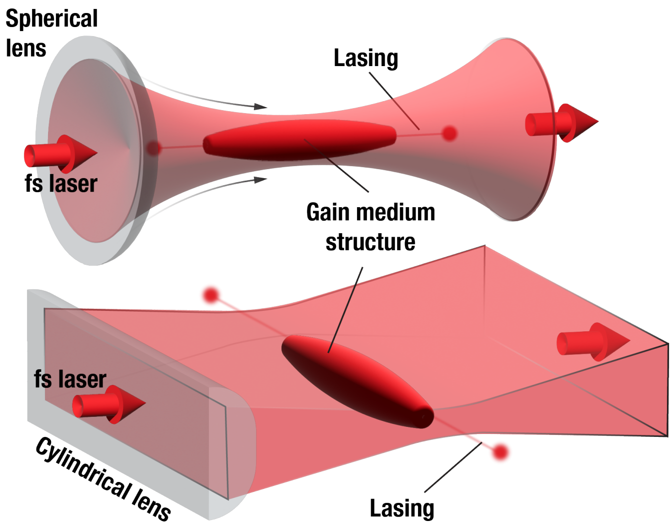

Figure 7: The gain medium generated by a spherical lens (above), and the gain medium generated by a cylindrical lens (below).

When using a spherical lens, the focus region will be along the same direction as the pump beam, thereby generating mirrorless lasing in the forward and backward direction, relative to the pump beam [1]. Because of this, mirrorless lasing generated in this way is known as either forward or backward lasing. If a cylindrical lens is used instead, the pump beam will become focused into a sheet. This will result in the gain region being located perpendicularly to the pump beam direction. The mirrorless lasing will then be generated perpendicularly relative to the pump beam. This process is known as sideways lasing [1].

Possible Emission Processes Responsible for Mirrorless Lasing

Mirrorless lasing is a broad concept that can include several phenomena [6]. The emission observed when performing mirrorless lasing has, in different research, been stated to be either ASE, superradiance, superfluorescence, or stimulated emission [6], [5]. Depending on the experimental conditions, different atomic phenomena can thus be observed. This implies that the spatial and temporal coherence of the emission can vary depending on the conditions of the experiment. The observed presence of coherence in several experiments suggests that mirrorless lasing could be a more advantageous laser diagnostic technique than LIF or TALIF for methods such as remote sensing [1]. This is due to the increased signal collection efficiency following the existence of coherence.

Previous research also suggests that the emission can transition from ASE to SF when performing mirrorless lasing [33]. If it holds that $T_2 \gg \sqrt{T_R t_D}$, then the emission will be SF [20]. If, on the other hand, it is true that $T_R \ll T_2 \ll \sqrt{T_R t_D}$, then ASE will be dominating the emission, since the coherence time is too short to allow a collective dipole moment to be built up. These relations, together with the definitions of these physical properties, suggest that by modifying the number of atoms N contributing to the generated field, or by altering the coherence time T_2, one can promote different emission processes.

2.3 Streak Camera Measurements

A streak camera is a type of fast detector used to image the propagation of light by generating a time-resolved image [34]. Using such a camera, it is thus possible to distinguish between different ultrafast events involving photons. The working principle of a streak camera is shown in Figure 8 below.

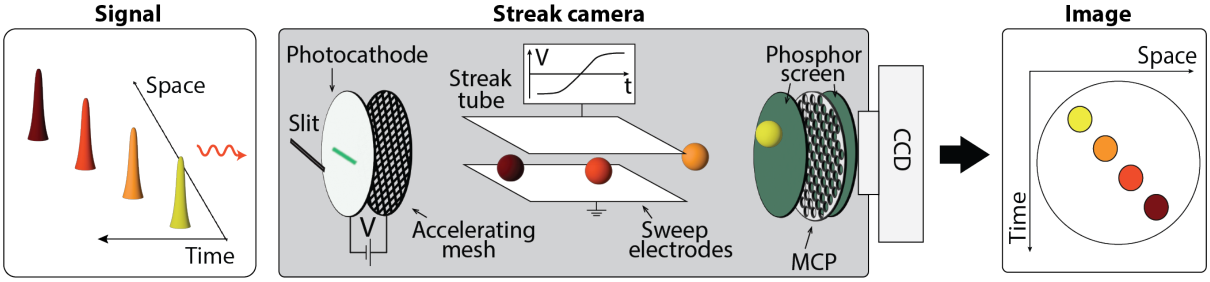

Figure 8: Graphics illustrating the different components of a streak camera and how the incoming signals can be temporally separated using the camera [34].

The photons reaching the streak camera will first pass through the slit and then hit the photocathode, where they are converted into electrons. These electrons will then be accelerated over a voltage applied between the photocathode and the accelerating mesh. They will then enter the streak tube, which consists of two sweep electrodes that sweep the voltage in time. Thus, the obtained deflection angle will vary depending on the arrival time. This mechanism thereby converts the temporal distribution into spatial. The separated electrons will then impinge on a phosphor screen, followed by a photocathode, and a microchannel plate (MCP), where the latter amplifies the signal. After hitting a second phosphor screen, the amplified electrons are converted back into photons, which can be recorded with a CCD camera. Finally, a time-resolved image can be obtained.

In order to obtain maximum temporal resolution, it is necessary to have a single stream of electrons passing through the sweep electrodes to ensure spatial separation on the CCD camera. Therefore, a minimised slit opening is required for high temporal resolution.

3 Method

3.1 Experimental Setup

The experimental goal for this project was to study mirrorless lasing in xenon gas, with a gain medium generated by two counter-propagating femtosecond laser pulses. The experimental setup is depicted with a 2D and 3D model in Figures 9 and 10, respectively.

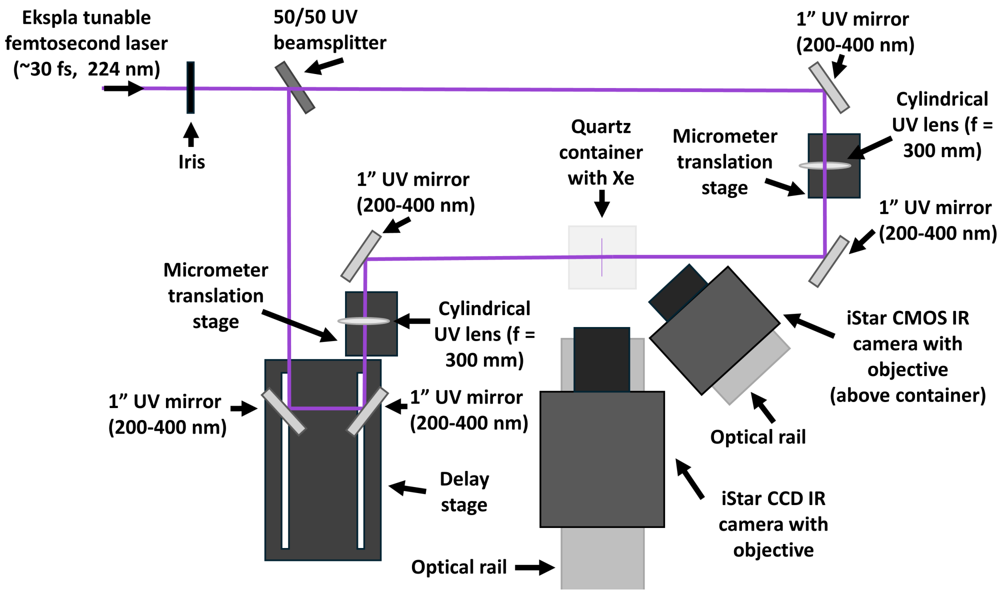

Figure 9: A top-down 2D model of the setup used to conduct the experiments. Note that the iStar CMOS IR camera is placed right above the quartz container in the actual setup. The angling of the camera is thus only made to facilitate the visibility of the setup.

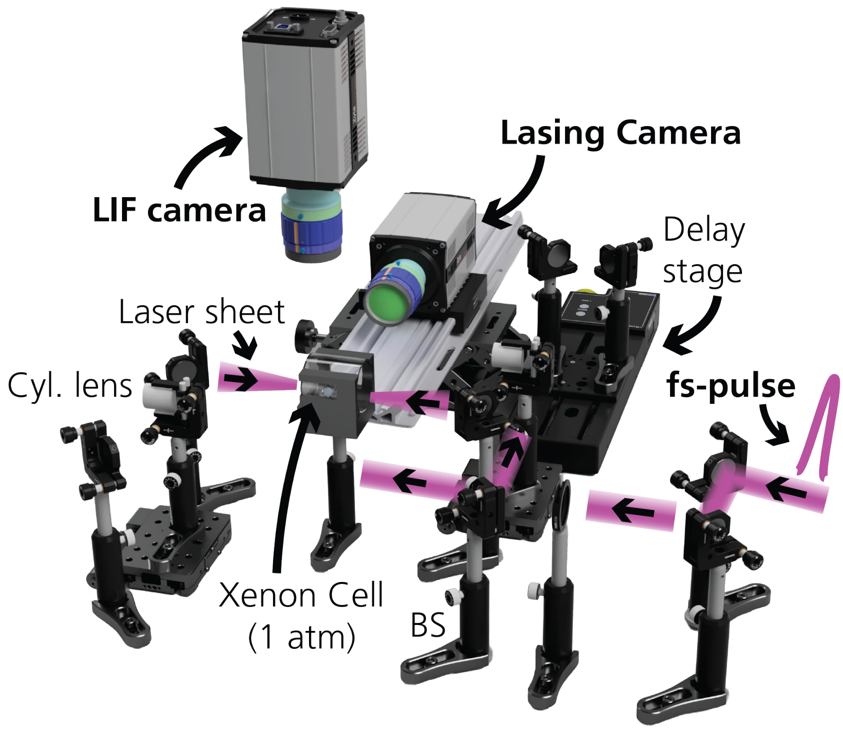

Figure 10: A 3D model of the setup used to conduct the experiments.

The pump laser used was a pulsed, tunable laser system from Ekspla (model FFL002), with a pulse length of around 30 fs and a beam width of circa 14 mm. The beam could be assumed to have a supergaussian shape. The wavelength used was the fourth harmonic of 896 nm, yielding a wavelength of 224 ± 1 nm. The pump laser is then passed through an iris, used for possible adjustments of the pump beam size and profile. A 50/50 beamsplitter was used to direct the pump beam along two different paths.

The reflected part of the beam was then reflected on two identical 1" UV mirrors placed on a motorised delay stage from Thorlabs. This made it possible to change the path length with micrometre precision, as displayed in both Figure 9 and 10. The pump beam then continued through a cylindrical UV lens with f = 300 mm, focusing the beam into a horizontal laser sheet. This lens was placed on a translation stage, making it possible to translate it manually with micrometre precision. Due to this choice of lens, the gain medium was assumed to generate sideways lasing. This type of lasing was chosen to fully separate the mirrorless lasing emission from the pump beam, thereby removing the need for filtering out the latter. Finally, the beam was reflected on another 1" UV mirror before entering the quartz container filled with xenon gas. Furthermore, the focus of the pump beam, generated by the lens, was adjusted to be at the centre of the container.

The other part of the beam, which was transmitted through the beamsplitter, reached a 1" UV mirror, which reflected it by 90 degrees so that it could pass through a cylindrical lens, identical to the one along the other path in the setup, and also placed on a micrometre translation stage. After being reflected at another 1" UV mirror, the beam reached the quartz container. Once again, the pump beam had its focus adjusted to the centre of the container, thereby ensuring that the beam waists of the two pump beams overlapped.

This setup was configured for the two separated beams to be counterpropagating. By having a delay stage inserted into one of the arms, it was possible to superimpose the beams both spatially and temporally. At a spatial overlap, the laser energy will roughly equal the energy of the beam exiting the laser, minus all the losses along the way. Due to an extra mirror along the delay arm, the energy along that path was always approximately 10 μJ lower. More generally, two counterpropagating photons can be seen to equal twice the energy of a single, identical photon [30]. If a temporal overlap is also achieved, the intensity at the overlap will be equal to twice that at the spatial overlap. Throughout the remainder of this thesis, the overlap will refer to the region where the beams are superimposed both spatially and temporally. Assuming that the relative angle between the two beams is negligible, the width of the overlap should be approximately equal to the length of the laser pulse itself. For a pulse duration of around 30 fs, this corresponds to a pump pulse width of $w = c \cdot 30$ fs ≈ 10 μm, with c being the speed of light in air. Assuming that the mirrorless lasing is emitted from the overlap, the width of the generated gain medium should be on the order of 10 μm. Since the foci of both beams are also located at the centre of the container, the highest intensity is ensured to be located at the overlap.

The transition probed for the Xe-atoms was from state $5p^6\ ^1S_0$ to $6p'[3/2]_2$, corresponding to a wavelength of 224.29 nm, for two-photon absorption [35]. A photon in the VUV regime would thus be needed to perform one-photon excitation for a similar transition, thereby motivating the need for two-photon absorption. Furthermore, the chosen transition is forbidden for a single-photon transition, making the use of two-photon absorption necessary. The atom then relaxed down to the 6s'$[1/2]^o_1$, during which it emitted photons with a wavelength of 834.68 nm. The atomic states involved thus correspond to a three-level system. An atomic gas was chosen over a molecular one since these have more well-defined energy states, making it easier to compare experimental measurements with theoretical predictions. The use of an atomic gas furthermore limits the impact of additional processes such as quenching, vibrational transitions, and rotational transitions.

The setup also included two iStar IR cameras with macroscopic objectives, one CMOS and one CCD. The CMOS camera was located directly above the quartz container, focusing onto the overlap of the two counterpropagating beams. This camera imaged the TALIF emission from the excited xenon gas, since this is emitted isotropically, yielding a good visualisation of the overlap. The CCD camera was located in the same plane as the beams, but perpendicularly to the pump beam path. This camera was used to image the sideways lasing signal. Depending on the experiment, the imaging devices were modified or altered in order to image different effects. Both cameras were mounted on optical rails, thereby making it possible to easily alter the imaging plane. The optical rail mounted to the CCD camera was also mounted to a LabJack. Through this configuration, it was possible to alter the height of that camera, thereby facilitating finding and centring the emission in the image plane of the camera.

3.2 Spatial Measurements

The first two experiments conducted with the setup described in Section 3.1 are centred around imaging the spatial characteristics of the observed TALIF and sideways lasing emission. The experiment described in Section 3.2.1 focuses on imaging and investigating the gain medium itself. The experiment described in Section 3.2.2 is instead centred around imaging the spatial evolution of the sideways lasing beam.

3.2.1 Imaging the Gain Medium

In order to image the sideways lasing emission at the location of the gain medium, the CCD camera was outfitted with a microscopic objective. The camera was then focused on the edge of the gain medium, and fixed at that position, where it could take high-resolution images of it. The pump laser was fixed at an energy of around 300 μJ. In order to visualise the gain medium geometry and compare the emission of TALIF to that of sideways lasing, the CMOS camera was set to image the TALIF emission from the gain medium simultaneously. Since TALIF is emitted isotropically, this imaging geometry was chosen purely for practical reasons, such as it yielding illustrative images of the overlap region.

Following the imaging of the gain medium at a single, fixed pump laser energy, the same experiment was repeated for different energies. By varying the pump laser energy, the power dependencies of the different types of emission were obtained. The pump laser energy was changed between 60 and 360 μJ. Recordings of the TALIF from outside the overlap, the TALIF from the overlap, and the sideways lasing resulted in three different power dependency studies.

3.2.2 Imaging the Sideways Lasing Emission Profile

For imaging of the sideways lasing beam profile, the CCD camera was moved along the optical rail. Initially, the macroscopic objective was set to focus on the gain medium. The camera was then moved away from the gain medium in steps of 20 mm, thereby mapping out the spatial evolution of the sideways lasing emission profile. During this displacement, the focus of the objective remained unchanged.

3.3 Temporal Measurements

The temporal characteristics of the sideways lasing emission were recorded by replacing the CCD camera with a streak camera. The streak camera was positioned in such a way that the sideways lasing emission entered at one of the sides of the slit. In order to measure the delay between the laser pump pulse and the sideways lasing emission, the laser was set to simultaneously emit the fundamental wavelength of 896 nm. Both the 896 nm beam and the sideways lasing beam were optically locked due to them being generated by the same laser system, guaranteeing that there was no jitter between the two beams. This wavelength was chosen since it was similar to the probed emission wavelength of Xe, and could therefore be recorded simultaneously with the streak camera.

By constructing a path with the exact same path length as one of the arms in the counterpropagating setup, the travel time for the fourth harmonic pulse was identical to that of the fundamental pulse, resulting in the latter accurately representing the pump pulse. The fundamental pulse was then directed, using optics, such that it impinged upon the other side of the streak camera slit. The streak camera measurements were performed with a streaking resolution of 10 ps/mm.

4 Results and Discussion

This section will present and discuss the results obtained with the experimental setup and methods described in Section 3. The structure of this section follows that of Section 3.

4.1 Spatial Measurements

The images in Figure 11 were acquired using the experimental method described in Section 3.2.1.

4.1.1 Imaging the Gain Medium

a)
b)

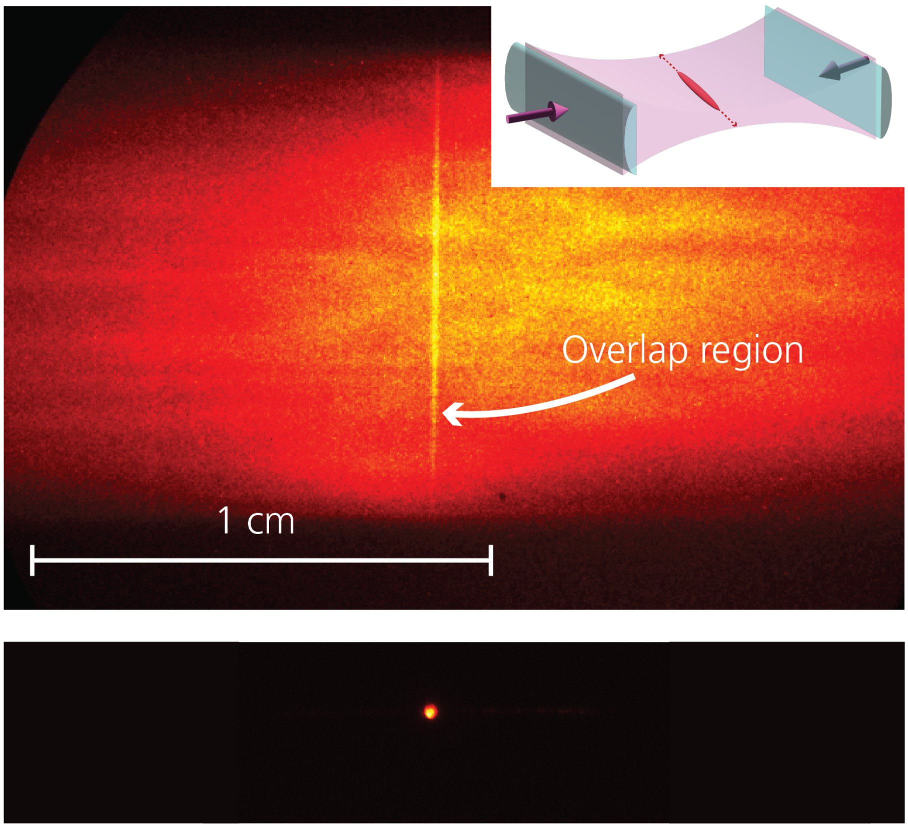

Figure 11: Images of the TALIF and sideways lasing at the gain medium. a) TALIF from xenon gas, imaged with the camera directly above the quartz container and focusing on the gain medium. The overlap volume is indicated by a sharp vertical intensity increase at the centre of the broad TALIF emission. b) Sideways lasing from xenon gas, imaged perpendicularly to the pump beam direction and focusing on the gain medium.

Imaging the TALIF Signal

The overlap of the counterpropagating beams is clearly visible in Figure 11a), as a vertical line of markedly increased TALIF intensity. It can be observed that the overlap region generally has a higher intensity compared to the regions where TALIF is generated without temporal overlap, due to the inherent non-linear intensity scaling of the

TALIF process: $I^2_{arm\ 1} + I^2_{arm\ 2} < (I_{arm\ 1} + I_{arm\ 2})^2$. Due to the choice of objective and image plane greatly affecting the obtained value, the observed width of the overlap could not be determined with certainty. It could, however, be concluded that the measured width was limited by the properties of the imaging device, rather than the actual width. More detailed measurements of this would require microscopic imaging with a higher resolution; however, for this work, we opted for a large field of view instead. When compensating for the chirp of the pump laser pulse, its experimentally obtained propagation length was on the order of 10 μm. We can then assume that the width of the overlap is of the same order of magnitude.

Imaging the Sideways Lasing Signal

The sideways lasing emission is shown in Figure 11b). Due to the use of cylindrical lenses to generate the gain medium, the mirrorless lasing was observed perpendicularly to the pump beam direction, thus qualifying as sideways lasing [5]. This result indicated that the direction of the mirrorless lasing emission can be modified by altering the gain medium geometry. The intensity of this emission was around a factor of 10^4 higher than the measured TALIF. Furthermore, the sideways lasing was observed to be highly localised in space. Both observations clearly suggest that the sideways lasing is not generated by TALIF, as TALIF lacks directionality. The observed emission is then concluded to be either stimulated emission, ASE, or SF.

The prominent localisation of the sideways lasing also indicates that a majority of the emission is from the overlap of the counterpropagating beams, rather than from the combined foci generated by the cylindrical lenses. The conclusion is motivated by the overlap being significantly less susceptible to intensity fluctuations along the pump beam, due to the thin gain medium imposing a hard restriction on the emission direction. This result then suggests that the gain medium is dictated by the overlap, thus further suggesting that the emission direction can be modified by changing the gain medium geometry. As stated, the intensity of the laser pump beam is twice as large at the overlap of the counterpropagating beams compared to outside it. This then implies that the gain medium consisted of the volume with the largest number of excited atoms, which aligns well with the theory described in Section 2.2.3.

Width of the Gain Medium

Width measurements similar to the ones conducted for the TALIF emission from the overlap were also made of the sideways lasing emission from the location of the gain medium. The same conclusions were drawn through similar observations, thereby suggesting a magnitude on the order of 10 μm for the sideways lasing emission right at the end of the gain medium. This then implies that the gain medium had a width roughly equal to this value. Using the theory described in Section 2.1.2, such a value would generate a Fresnel number of the following size,

$$F = \frac{\pi w^2}{L\lambda} = \frac{\pi \cdot (\sim 5\ \mu\text{m})^2}{1\ \text{cm} \cdot 834.68\ \text{nm}} \approx 9 \cdot 10^{-3} \ ,$$

which indeed is significantly smaller than one. This relation is assumed to hold for all measurements described in the subsequent parts of this report.

Intensity Dependence of the TALIF Signal on Pump Laser Energy

The measured intensity as a function of laser intensity is shown in Figure 12 for the TALIF emission from outside the overlap region and from the overlap.

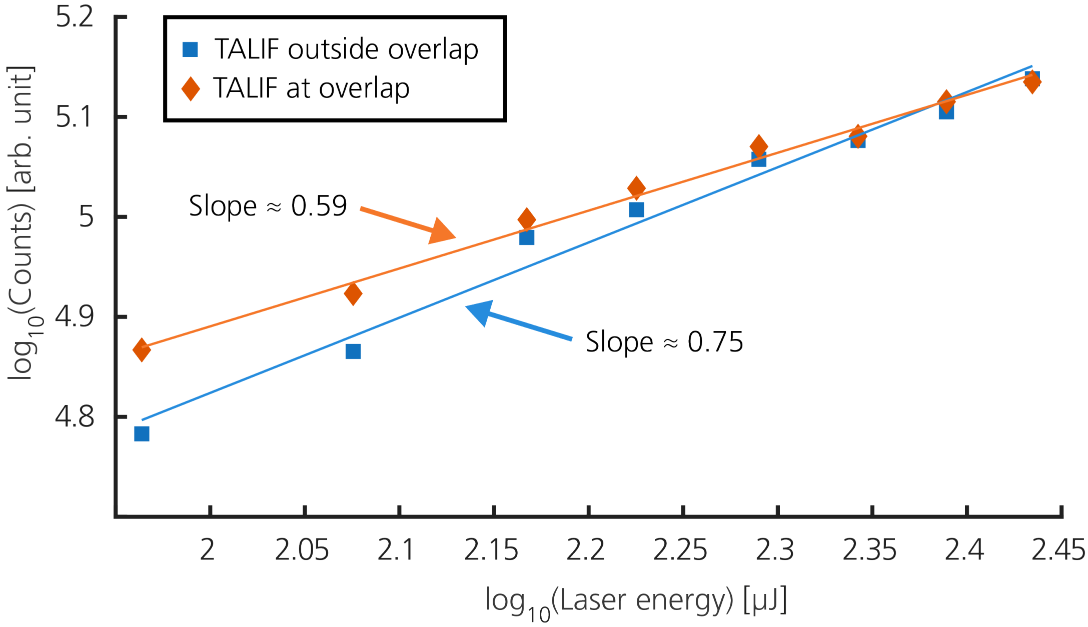

Figure 12: Power dependency graphs for the TALIF emission from the region outside the overlap (blue) and from the overlap of the beams (orange). The solid lines in corresponding colours are linear fits for the two sets of data points. The slopes of these lines correspond to the relation between the pump laser intensity and the TALIF signal intensity on a logarithmic scale.

As stated in Section 2.2.2, TALIF emission grows proportionally to the intensity of the pump laser squared. This implies that the solid lines in Figure 12 should have slopes equal to two, since the plots displayed in the figure are on a logarithmic scale. This is, however, not the case; the TALIF from outside the overlap grows with a rate of 0.75, while the TALIF from the overlap grows with a rate of 0.59. The observed deviation can be explained by the system having reached a partially saturated state [3].

The partially saturated regime of an atomic system yields a TALIF signal which displays an asymptotic behaviour. Weak pumping will result in the system being in a linear regime, corresponding to $N_{ex} \propto I_p^2$ for TALIF, with N_{ex} being the number of excited atoms and I_p being the pump laser intensity. However, stronger pumping will lead to a decrease in the growth of N_{ex} until finally reaching a plateau. Since the observed slopes are between zero and one, it can be assumed that the system has been partly saturated. This assumption is plausible since the pump laser beam has a peak power of around 3 GW for an energy of 100 μJ. Despite the high intensity, it is still reasonable that full saturation has not been achieved. This can be motivated by several factors decreasing the excitation efficiency. These include the pump wavelength being in the UV range, where we do not have extreme energies to work with, TALIF having a generally low absorption cross section, and the pump laser having a supergaussian shape [30].

The assumption that a partly saturated state has been reached is further motivated by the slope of the TALIF from the overlap being lower than that from outside the overlap. The beamsplitter included in the setup described in Section 3.1 splits the pump laser beam into two parts with roughly equal intensities. This implies that the intensity of the pump laser beams at the overlap is approximately twice as large as the intensity outside the overlap. It is then logical that the overlap region should be closer to complete saturation. Additionally, an intensity being twice as high suggests, according to Section 2.2.2, that the TALIF emission from the overlap should then be around a factor of four larger than that from outside the overlap. However, it should be noted that the intensity difference never exceeds approximately 1.2. A possible explanation for the observed discrepancy could be that TALIF and sideways lasing are competing processes of emission. This suggestion is motivated by both emissions corresponding to a relaxation between the same atomic states. Due to the overlap yielding the clear majority of sideways lasing emission, it is possible that this results in decreased TALIF intensity from that region. Additional measurements would, however, be needed to verify this conclusion.

Intensity Dependence of the Mirrorless Lasing Signal on Pump Laser Energy

Figure 13 illustrates how the intensity of the observed sideways lasing depends on the pump laser energy. The emission can be seen to have a clear threshold. It can thus once again be concluded that the detected sideways lasing is not spontaneous emission, emitted as TALIF. This behaviour also suggests that the number of excited atoms has to be sufficiently high for mirrorless lasing to be detected.

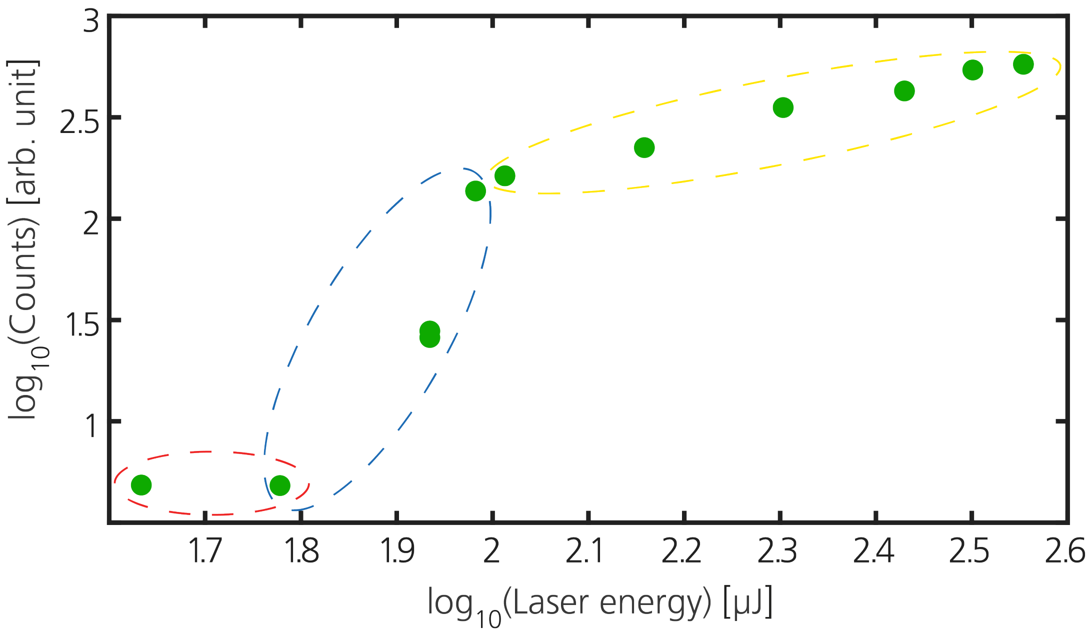

Figure 13: Power dependency graph for the sideways lasing emission on a logarithmic scale. The three dashed ellipses correspond to the different regimes observed. The red ellipse indicates the threshold regime, the blue the linear regime, and the yellow the plateau regime.

According to Section 2.1, three of the four described types of emission yield signals include a threshold: stimulated emission, ASE, and SF. Furthermore, Equation (6) shows that the number of excited atoms is required to be large in order to observe ASE, rather than spontaneous emission, since a positive population inversion ΔN is needed to fulfil that condition. For SF to be generated, the number of atoms initially excited, N, must be even larger than in the ASE case. This is motivated by $T_R \ll T_2 \ll \sqrt{T_R t_D}$ needing to hold for SF to be observed. If this is not the case, ASE will be generated instead.

The data points shown in Figure 13 indicate that there are different emission regimes. These are emphasised by the dashed ellipses in the plot. This conclusion was also drawn in previous research on sideways lasing by Dominguez et al. (2025). The first, consisting of the points enclosed in the red ellipse, is the already discussed threshold regime. Following that, the data points in the blue ellipse display an approximately linear increase. This suggests that the observed emission is neither stimulated emission nor ASE, since both have quadratic dependencies of the pump laser intensity for two-photon excitation when expressed on a logarithmic scale, according to Equations (4) and (6). However, for the case of two-photon excitation, the intensity of SF, I_{SF}, should depend on the pump laser intensity as $I_{SF} \propto I_p^4$, according to Equation (10). In the logarithmic plot, which is Figure 13, this should be illustrated as a linear growth with a slope of four. Since a linear regime can be found in Figure 13, SF seems to be the emission that is in best accordance with the obtained data.

The regime following the linear, indicated by the yellow ellipse, involves growth at a slower rate. This is therefore called the plateau regime. The behaviour can be credited to other atomic processes being more significant at higher pump laser energies. Examples of such processes are photoionisation and Stark shifts. Photoionisation involves the excited electron escaping from the system rather than relaxing to a lower state by emitting a photon [3]. Stark shifts are shifts of the atomic energy states due to a strong external field, resulting in the frequency of the pump photons not being equal to the new resonance frequency [7].

4.1.2 Imaging the Sideways Lasing Emission Profile

Figure 14 shows a three-dimensional reconstruction of the sideways lasing beam over a distance of 160 mm, as well as a plot depicting the changes in intensity over distance.

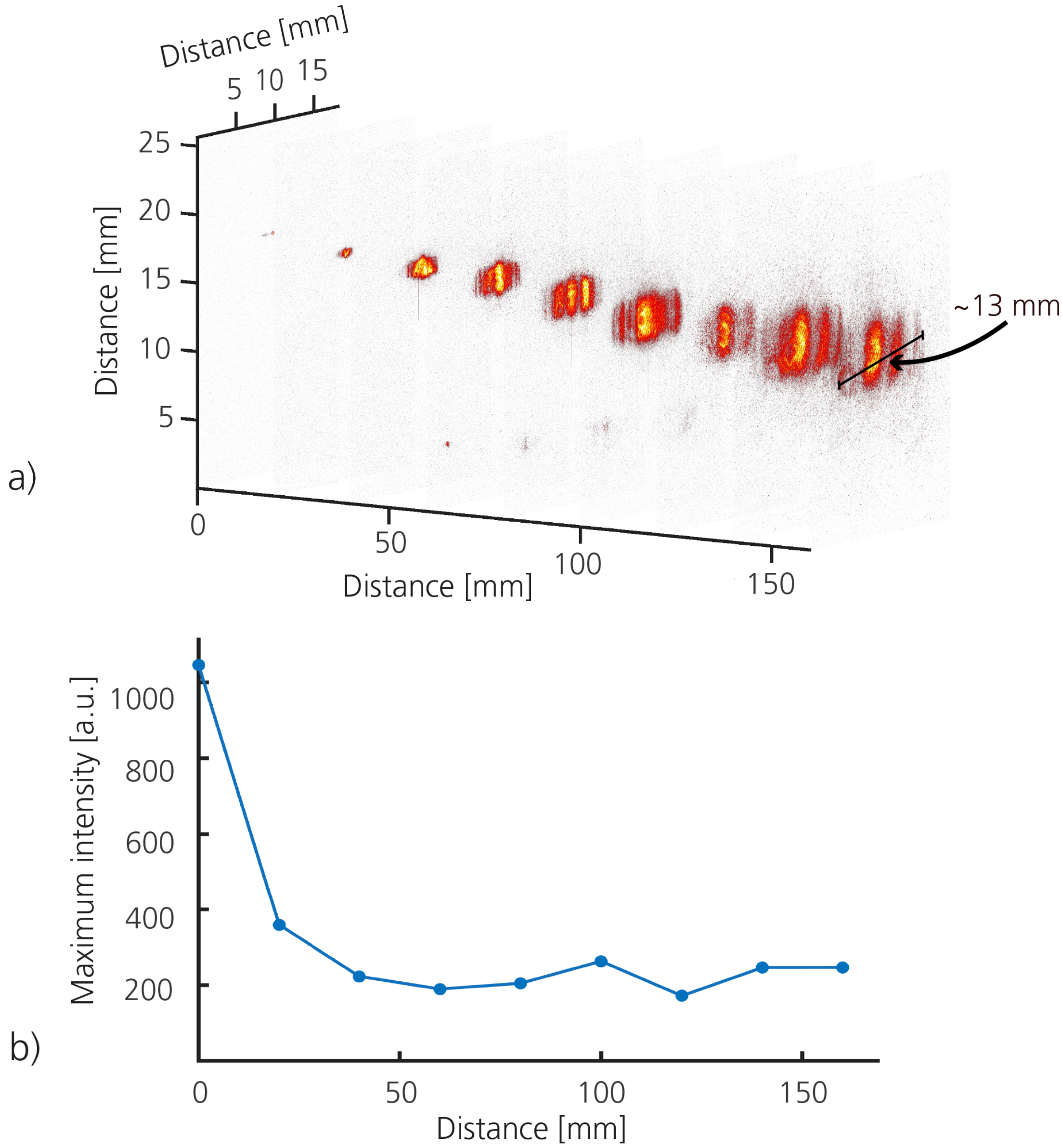

Figure 14: Illustrations of the beam profile of sideways lasing. a) A 3D reconstruction of the beam profile measured over a total distance of 160 mm. Starting with focusing directly on the gain medium, the camera was moved, and images of the beam were acquired with a 20 mm spacing. Note that each image is normalised to itself, rather than to the others. b) Plot showing the changes in maximum intensity of the sideways lasing emission as a function of distance.

The emission is clearly confined to a direction perpendicular to the pump beam, thus further proving that the observed mirrorless lasing is sideways lasing. Comparing the beam profile at the location of the gain medium to locations further away in Figure 14a), it is clear that the beam diverges significantly. This observation aligns well with predictions for geometries with $F \ll 1$ described in Section 2.1.2, where it is stated that the diffraction should be pronounced for such geometries.

The plot in Figure 14b) displays how the maximum sideways lasing intensity changes with distance. The maximum intensity decreases sharply over a distance of circa 40 mm from the focus. As the distance increases, the maximum intensity is observed to average out to a roughly constant value. This can be explained by the beam being distinctly divergent, and thus expanding much more rapidly near the beam focus, here corresponding to the gain medium, than farther from it.

Calculation of Beam Divergence

There are two different angles describing the behaviour of the beam profile over a distance, the diffraction angle θ_D describing the predicted Fraunhofer diffraction pattern, and the divergence angle θ_{div}, describing the extension of the spatial profile. The latter can be related to the diffraction pattern, through $2 \cdot \theta_D$ being the spatial extension of the first-order diffraction. However, the divergence of the beam can also be calculated using that $\theta_{div} = 2 \cdot \tan^{-1}(z/d)$, where z is the diameter of the beam at a chosen location and d is the distance from the end of the gain medium to that location.

Figure 15 displays the beam at a distance of 160 mm from the gain medium. Measuring the beam profile using this image yields a total transverse width of circa 13 mm.

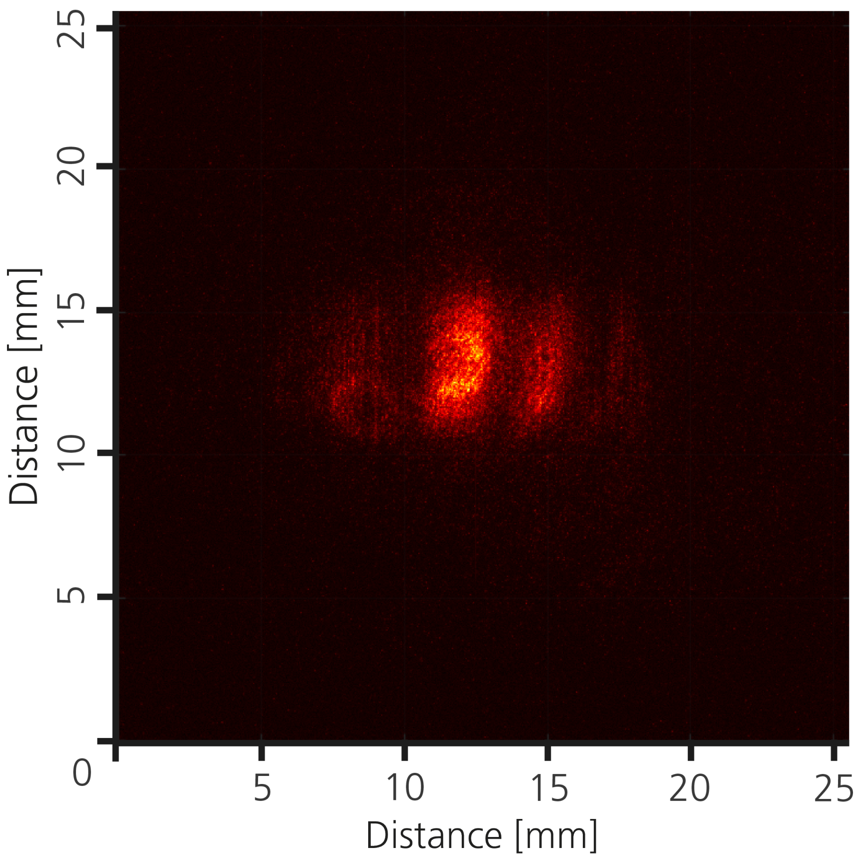

Figure 15: Image of the beam 160 mm from the gain medium.

The measured values give a divergence angle of approximately $\theta_{div} = 2 \cdot \tan^{-1}$ (13 mm/160 mm) $\approx 5°$. Using the emission wavelength and width of the gain medium, the first order of diffraction has a divergence angle equal to $\theta_{div} = 2 \cdot \theta_D = 2 \cdot \sin^{-1}(834.68\ \text{nm}/9\ \mu\text{m}) \approx 10°$. This shows that the measured divergence is significantly smaller than the predicted one. Such a deviation could imply that the observed ring pattern is due to a behaviour other than Fraunhofer diffraction. Because the pump pulse has a supergaussian shape, it is highly likely that the observed pattern is instead due to interference between transverse variations in absorbed radiation. Previous research by Dominguez et al. (2025) yielded a multi-modal beam expansion of 66°, for a gain medium width of 4 mm and $F \gg 1$. These results show that a narrow gain medium with a single mode provides more directed emission than multi-modal emission.

Evidence of Single Mode Emission

The theory presented in Section 2.1.2 predicts that a gain medium with $F \ll 1$ will generate a clear diffraction pattern, since only one mode is present in this geometry. However, the conclusion made in the paragraph above states that the pattern of rings observed in Figure 15 is due to interference rather than diffraction. The shape of the observed pattern is in good accordance with theory, since the gain medium is roughly cylindrical and thereby is assumed to yield an approximately circular interference pattern. The clear evidence of interference indicates that the emission is indeed both temporally coherent and generated by a single transverse mode; further strengthening the assumption that $F \ll 1$ for the gain medium, as well as suggesting that the emission is stimulated emission or SF, rather than ASE. It can then be assumed that $T_2 \gg \sqrt{T_R t_D}$ holds for the experiment in this project, if the emission is proved to be SF. This indicates that the number of atoms contributing to the generated field N is large enough for T_R to be significantly shorter than T_1.

The recorded emission in Figure 15 also shows large variations in intensity transversely across the beam, which cannot be credited to the diffraction pattern. Since sideways lasing is strictly dependent on the atoms generating the gain medium, an uneven distribution of excited atoms could lead to an uneven beam profile. The pump laser beam profile does exhibit intensity variations owing to nonlinear optical effects, such as self-phase modulation during propagation towards the sample. The intensity variations across the sideways lasing beam could then be explained by the uneven excitation. Furthermore, despite the clear majority of the sideways lasing being generated by the overlap, a small amount is also generated solely by the focused pump laser pulse outside the overlap. Interference between this emission and that from the overlap could also possibly explain the observed intensity variations in Figure 15. However, experiments optimised for studying this effect would have to be performed in order to provide a reliable conclusion.

4.2 Temporal Measurements

The pump laser pulse and the following sideways lasing emission were temporally resolved using the method described in Section 3.3. An image of a single-shot measurement of the two pulses observed, and the corresponding temporal plot is shown in Figure 16.

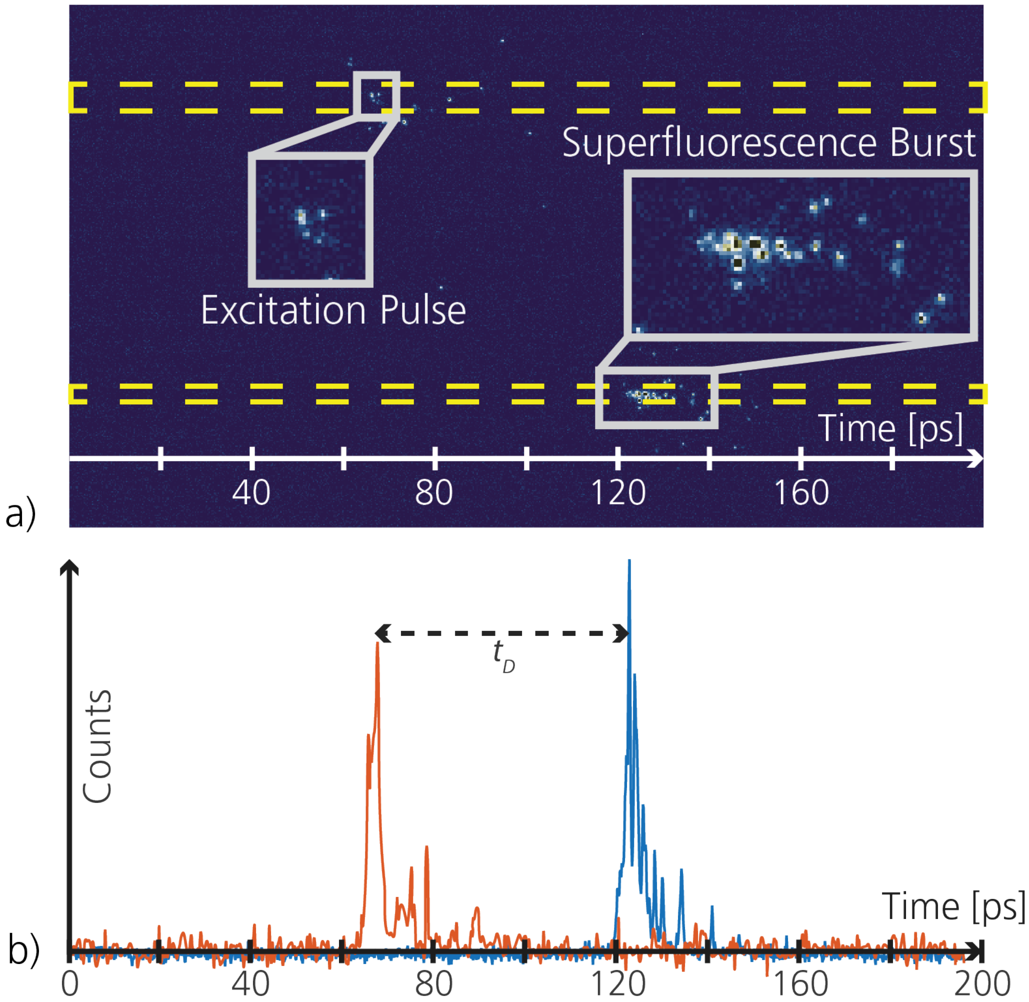

Figure 16: Image and plot illustrating the temporal evolution of the pump laser pulse and following sideways lasing emission. a) Single-shot image of the pump laser pulse (excitation pulse) and the sideways lasing emission (superfluorescence burst). b) Plot of intensity counts over time. Curves showing the temporal evolution of the pump laser pulse (orange), as well as the sideways lasing emission (blue).

The Relation Between the Excitation Pulse and Sideways Lasing Pulse

A clear delay of circa 70 ps between the pump laser pulse and the sideways lasing emission can be observed. This observation indicates that the sideways lasing emission is not pure stimulated emission since this occurs while the pump pulse is still present. The temporal evolution of ASE does involve a delay in the form of the propagation time through the gain medium t_p. This value corresponds to a duration of circa 47 ps for this experiment, since the sample has a length $L = 14$ mm. However, this value does not fully account for the measured delay between the pulses. This suggests that the physical process behind the observed sideways lasing emission cannot be ASE either. The SF process does include a clear delay t_D between the excitation pulse and the subsequent emission. According to Section 2.1.2, these values are on the order of tens of picoseconds for atoms and molecules in the gas phase, which is the case for the gain medium used in this experiment. The observed delay thus aligns well with the definitions of SF.

The Temporal Shape of the Sideways Lasing Pulse

The detected sideways lasing exhibits a clear pulse shape with a sharp rise. The shape corresponds to the described emission behaviour of SF, where a collective dipole moment is built up from weak quantum fluctuations, which results in the gradual emission of photons. The sharp increase in intensity is in agreement with the theoretical descriptions of SF, since these suggest that $I_{SF} \propto N^2$, where I_{SF} is the intensity of the SF emission and N is the number of atoms contributing to the generated field. The shape of the pulse can be considered to be similar to both the predicted sech^2 function and Bessel functions; however, further measurements have to be performed in order to verify if this is the case.

Figure 16 yields a superradiance time T_R on the order of tens of picoseconds. This is significantly lower than previously measured values of T_1 for two-photon excitation of xenon, which were around 100 ns [36]. The obtained value thus suggests that N is considerably high, which aligns well with previous conclusions from this experiment. The measured sideways lasing pulse also displays oscillations on the decline. This indicates that the emission is similar to the theoretical predictions of mirrorless lasing emission from a gain medium with $F \ll 1$, shown in Figure 3. However, due to the image being single-shot, it is difficult to draw any firm conclusions regarding the observed oscillations.

The Behaviour of the Averaged Sideways Lasing Pulse

An average of several temporal single-shot measurements is displayed in Figure 17.

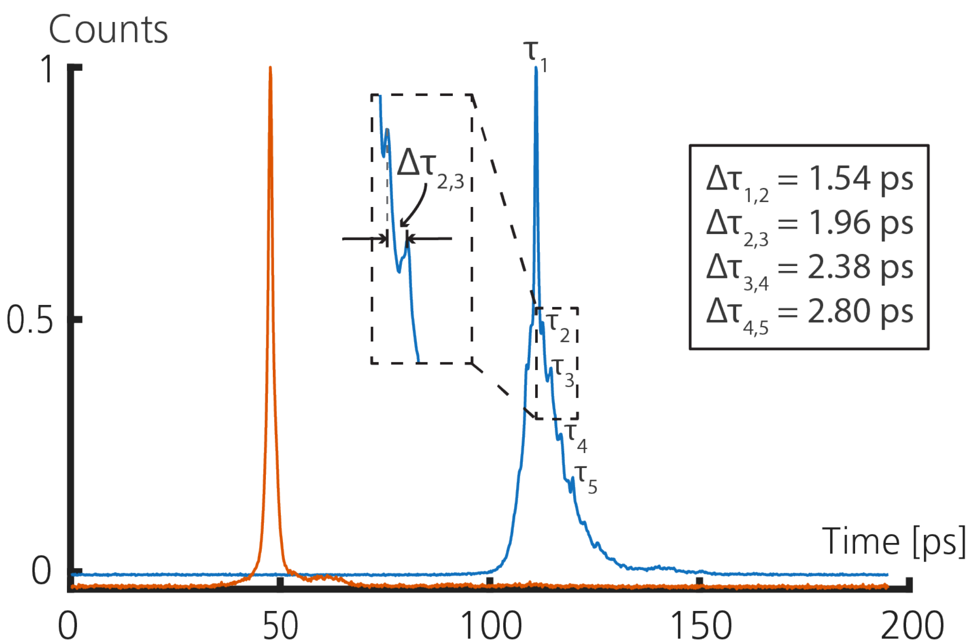

Figure 17: Averaged temporal plots of the pump laser pulse (orange) and the sideways lasing emission (blue). The list of $\Delta\tau$ values corresponds to the differences in time between the oscillations during the decay of the pulse. For example, $\Delta\tau_{2,3}$ corresponds to the difference in time between the third peak located at τ_3, and the second peak located at τ_2.

The pump laser pulse can be seen here to have a distinct shape similar to a supergaussian, with minimal noise. Similarly to Figure 16, there is a clear delay time between the pump pulse and the subsequent sideways lasing emission. The sideways lasing emission still shows a drastic increase in intensity; however, the averaging of single-shot data resulted in a broadening of the pulse. This effect indicates that t_D may fluctuate across measurements.

The recorded sideways lasing emission shows oscillations in the temporal signal, both on the incline and decline of the pulse evolution. The oscillations persist despite averaging, suggesting they are not caused by noise but have a physical significance. SF displays clear oscillatory behaviour on the decline of the pulse for gain media with $F \ll 1$, which is the case for the gain medium used in this experiment. The oscillations observed on the decline in Figure 17 can therefore be credited to Rabi oscillations of the generated field, according to the theory described in Section 2.1.2. As a result, the oscillation frequency should decrease over time as light leaks out of the gain medium. Figure 3 shows a theoretical prediction of this behaviour. The time differences $\Delta\tau$ in Figure 17 show a clear increase over time, thereby suggesting that the frequency of the oscillations is indeed decreasing. It should be noted that the streak camera used had a streaking resolution of 10 ps/mm, with a maximum overall resolution of 1.9 ps [34]. This implies that the shape of the recorded oscillations cannot be completely trusted. Considering all of these conclusions, the measured pulse can be seen to be in very good agreement with the prediction for SF in Figure 3.

According to Section 2.1.2, SF also displays oscillations on the pulse's incline for large values of N. This condition is satisfied for this experiment, as described in the paragraph above regarding the temporal shape of the sideways lasing pulse. The large value of N can be explained by the excitation being performed with a laser pulse having a peak power with a magnitude of a few GW. It can thus be concluded once again that the theory for SF aligns very well with the obtained results.

The Dependency of the Sideways Lasing Pulse Delay on Pump Laser Energy

Figure 18 illustrates the dependency of t_D on two different physical quantities; pump laser energy and vacuum-field fluctuations. Measurements of t_D while increasing pump laser energy in approximately equal increments of $\sim$30 μJ, yielded the plot shown in Figure 18a).

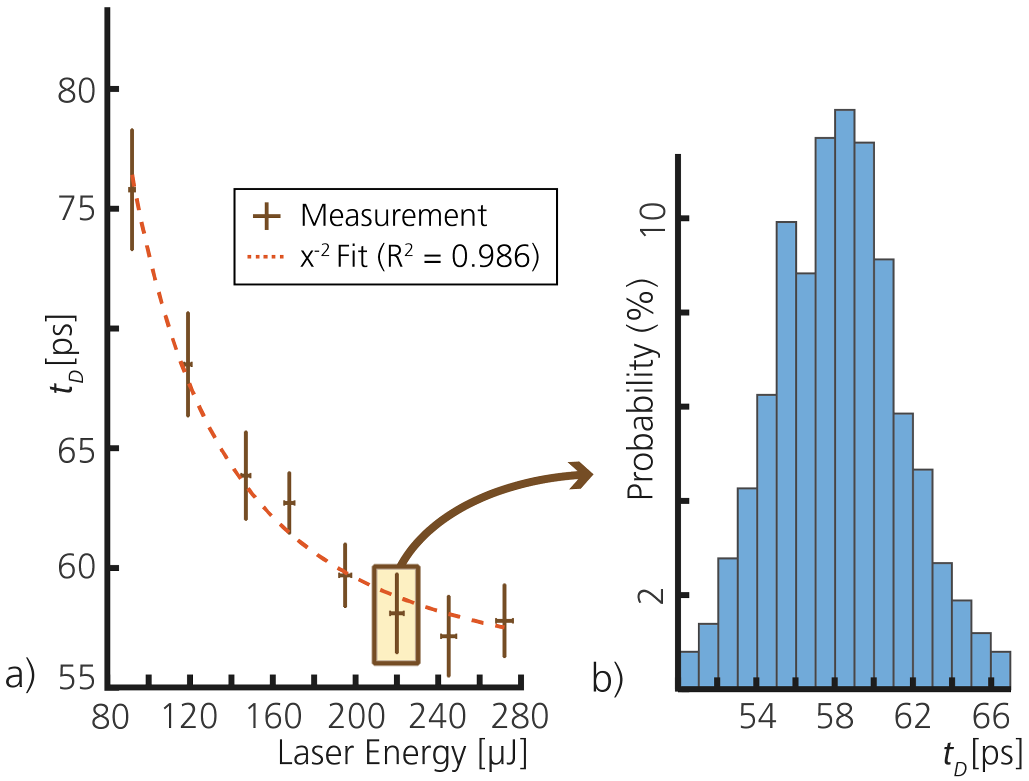

Figure 18: Plots depicting different variations of t_D. a) Plot illustrating how the value of t_D changes with pump laser energy. b) Histogram showing the random variations in t_D for a pump laser intensity of 220 μJ.

According to the figure above, t_D clearly decreases with increasing laser energy. The made observation aligns well with the predicted behaviour described by Equation (11). Due to the pump laser beam exciting the atoms through two-photon absorption, the number of atoms contributing to the generated field relates to the pump laser intensity through $N \propto I_p^2$. This yields that $t_D \propto E_p^{-2}$, where E_p is the pump laser energy, assuming a constant pump beam size at the location of excitation. A fit performed on the data shown in Figure 18a), corroborates the prediction and yields an R^2-value of circa 0.986. According to Equation (11), t_D is proportional to T_R. This implies that a similar behaviour of T_R should be observed for increasing laser energies.

Quantum Fluctuations of the Sideways Lasing Pulse Delay

The histogram shown in Figure 18b) indicates the probability distribution of t_D, for a pump laser energy value of 220 μJ. As stated in Section 2.1.2, the value of t_D also depends on the initial angle of the macroscopic Bloch vector θ^i. The size of this angle depends on the number of atoms initially decaying through spontaneous emission, which occurs due to vacuum-field fluctuations. Therefore, the variations of t_D for a single pump laser energy should be caused by variations of the vacuum-field fluctuations. This furthermore suggests that variations in the vacuum-field can lead to variations of t_D on the order of $\pm$9 ps, according to the range of t_D-values shown in Figure 18b). Due to the width of the sideways lasing pulse imaged with a single shot in Figure 16 being around 10 ps, while the averaged pulse width in Figure 17 being around 20-30 ps, the observed broadening could be explained by the variations in t_D.

5 Conclusion

In this thesis project, mirrorless lasing was investigated in both fundamental and applied contexts. First, a setup containing counterpropagating femtosecond pulses was built, such that a gain medium with $F \ll 1$ and a sideways emission direction was obtained. With this gain medium, power dependency scans were performed in order to study the emission behaviour. Following that, the emission profile was measured with the purpose of further investigating which physical process was responsible for the sideways lasing emission. Finally, temporal measurements were performed to detect the quantum mechanical behaviour of the system. The results show that the observed sideways lasing indeed is superfluorescence (SF). We were able to connect many of the experiments directly to both the fundamental generation of SF and various gain medium predictions for it. This also implies that the emission direction can be easily modified by altering the geometry of the gain medium.

The first goal of this project was to investigate how the mirrorless lasing emission depended on the gain medium geometry. Observations clearly indicate that the gain medium in a gaseous sample can be effectively controlled. It was shown to consist almost solely of the volume experiencing the highest pump laser intensity, suggesting that it can be easily modified by changing the excitation geometry. Furthermore, the generated sideways lasing was observed in the predicted direction, demonstrating good agreement with theory and previous research and suggesting that the emission direction can be readily altered.

The second goal was to discover which light-matter interaction is responsible for the sideways lasing emission. The conducted measurements of the spatial and temporal dependencies on power and geometry all indicated that the atomic process generating the sideways lasing was indeed superfluorescence (SF). The expansion of the beam was also significantly smaller than that of the multi-modal emission recorded by Dominguez et al. (2025). This conclusion is promising, since it suggests that highly directional, single mode, sideways lasing is possible. Recordings of the beam profile in the far field displayed an interference pattern, further suggesting that the sideways lasing was both coherent and single mode, once again aligning with the predictions for SF.

Power-dependence measurements were made for both the incoherent and isotropic Two-photon Absorption Laser Induced Fluorescence (TALIF) emission and the coherent, directional sideways lasing emission. The former deviated from theoretical predictions, showing clear signs of reaching a saturated state. This is a reasonable conclusion given the pump laser's high peak power. However, the sideways lasing yielded a power dependence with a clear threshold and a linear regime, aligning well with predictions of the intensity behaviour for SF.

Streak camera recordings of the pump laser signal and sideways lasing emission further supported that SF is the dominant process within these experiments. The sideways lasing exhibited a narrow pulse shape, recorded with a delay of approximately 70 ps relative to the pump pulse. The only relevant emission process capable of generating delay times of that magnitude is SF. Additionally, the measured dependence of t_D on the pump laser energy was very similar to the predicted behaviour for this emission process. Oscillations were also measured on both the incline and the decline of the pulse, with the frequency of the latter decreasing over time. These observations align very well with the predicted pulse shape for SF with a gain medium having $F \ll 1$.

All in all, the results in this project clearly show that it is possible to generate cavity-free, coherent emission with an intensity several orders of magnitude stronger than TALIF in the form of mirrorless lasing. It can also be concluded that this emission is SF when xenon gas is excited with an ultrafast laser, further showing that it can be generated at 1 atm. Thus, contrary to previous research by Maki et al. (1989), it does not seem necessary to use ultracold atoms to generate SF if excitation is performed at sufficiently high peak powers, attainable with femtosecond excitation. These conclusions suggest that mirrorless lasing is a highly promising method for laser diagnostics.

6 Outlook

Given the promising results of this project, many additional experiments could be highly beneficial. The dependence of sideways lasing on the gain medium geometry was thoroughly studied in this project. However, this relation could be investigated even more rigorously. According to research by Gross and Haroche (1982), minimal divergence of emitted SF is obtained when the gain volume has dimensions yielding $F \approx 1$. A potential future experiment would thus involve reshaping the gain medium to achieve such a geometry. This can experimentally be performed in several ways. Altering the chirp of the pump laser pulse would extend the pulse duration, thereby increasing the overlap of the counterpropagating pulses. This would then equal an increase in the gain medium width. By using an adjustable slit or iris placed before the beamsplitter in the experimental setup, the width of the pump laser pulse can be manually adjusted. Such alterations would change the length of the gain medium. Using these types of modifications, it should be possible to achieve a gain medium geometry with $F \approx 1$.

For a more advanced possible modification of the gain medium, one could structurally modulate the pump laser beam. This could be achieved by letting the pump beam propagate through a DOE or Ronchi ruling, which imposes intensity variations across the beam, thus creating many gain volumes in a row. Such a modulation of a mirrorless lasing gain medium, resulting in a nonuniform intensity distribution, could give additional information in both the spatial and temporal domains.

The spatial measurement described in Section 4.1.1 could, with advantage, be executed again with a modified experimental setup. As stated, it was not possible to fully resolve the gain medium with the used setup. Changing the imaging equipment or the measurement technique entirely could yield more accurate dimensions, which, in turn, could provide highly advantageous information for comparing experimental data with theoretical predictions.

An additional future study is to perform a series of measurements where the value of N, i.e., the number of atoms contributing to the generated field, is varied by changing the xenon concentration in the cell. Such a study would yield a thorough analysis of the temporal evolution of sideways lasing, since T_R, t_D, and the intensity of the SF signal all depend on N. According to theory, lowering N would cause the sideways lasing to transition from SF to ASE and, ultimately, to spontaneous emission. Observing such a transition would further establish which physical process underlies mirrorless lasing and how this emission can be controlled.

Performing theoretical modelling of the sideways lasing would yield additional valuable information. Such work could investigate if the sech^2 function, a combination of Bessel functions, or another mathematical function, is best suited to describe the intensity evolution over time for the recorded sideways lasing. Since the sideways lasing was found to be SF in this project, such modelling could provide useful information by connecting the theory in Section 2.1.2 to the experimental results.

The future goal of this research is for mirrorless lasing to be an emission characterised thoroughly enough to be used as a laser diagnostic method. While the ultimate goal can be considered to be using mirrorless lasing in remote sensing, there are other applications that are more readily achievable. The same experiments conducted in this project can, with advantage, be performed on other atomic species found in gases or laminar flames. Other applications of interest include measuring molecular species and different plasma formations.

All in all, to the best of the author's knowledge, these types of measurements made on mirrorless lasing, with a gain medium of $F \ll 1$ and a gas at atmospheric pressure, have never been performed previously. This thesis therefore provides a start to a field of research in which mirrorless lasing can become a viable optical diagnostics method, to be used where strong, directional emission is required.

References

[1] Dominguez A, Ravelid J, Raveesh M, Hosseinnia A, Ehn A, Bood J. Spatial characterization of sideways lasing. Optics Express. 2025;33(12):25261-74.

[2] Dogariu A, Michael JB, Scully MO, Miles RB. High-gain backward lasing in air. Science. 2011;331(6016):442-5.

[3] Eckbreth AC. Laser diagnostics for combustion temperature and species. Gordon and Breach Publishers; 1996.

[4] Ramaswamy A, Chathanathil J, Kanta D, Klinger E, Papoyan A, Shmavonyan S, et al. Mirrorless lasing: a theoretical perspective. Optical Memory and Neural Networks. 2023;32(Suppl 3):S443-66.

[5] Miles RB, Dogariu A. Backward, forward and around the corner lasing in air. In: AIAA AVIATION 2020 FORUM; 2020. p. 3239.

[6] Nastishin YA, Dudok TH. Optically pumped mirrorless lasing. A review. Part I. Random lasing. Ukrainian Journal of Physical Optics. 2013;14(3):146-70.

[7] Foot CJ. Atomic physics. vol. 7. Oxford University Press; 2005.

[8] Saleh BEA, Teich MC. Fundamentals of photonics, 2 volume set. John Wiley & Sons; 2019.

[9] Milonni PW. An introduction to quantum optics and quantum fluctuations. Oxford University Press; 2019.

[10] Tihon D, Withington S, Bailly E, Vest B, Greffet JJ. General relation between spatial coherence and absorption. Optics Express. 2021;29(1):425-40.

[11] Dolezal J, Sagwal A, de Campos Ferreira RC, Svec M. Single-molecule time-resolved spectroscopy in a tunable STM nanocavity. Nano Letters. 2024;24(5):1629-34.

[12] Ghani Moghadam G, Farahbod AH. General formula for calculation of amplified spontaneous emission intensity. Optical and Quantum Electronics. 2016;48(4):227.

[13] Filatov S, Auzinsh M. Towards Two Bloch Sphere Representation of Pure Two-Qubit States and Unitaries. Entropy. 2024;26(4):280.

[14] Wang XR, Zheng YS, Yin S. Spin relaxation and decoherence of two-level systems. Physical Review B. 2005;72(12):121303.

[15] Chen Y, Peng S, Fu Z, Qiu L, Fan G, Liu Y, et al. Ultrafast quantum control of atomic excited states via interferometric two-photon Rabi oscillations. Communications Physics. 2024;7(1):98.

[16] Feng N, Lu M, Sun S, Liu A, Chai X, Bai X, et al. Light-Emitting Device Based on Amplified Spontaneous Emission. Laser & Photonics Reviews. 2023;17(7):2200908.

[17] Liao R, Mei C, Song Y, Demircan A, Steinmeyer G. Spontaneous emission noise in mode-locked lasers and frequency combs. Physical Review A. 2020;102(1):013506.

[18] Gross M, Haroche S. Superradiance: An essay on the theory of collective spontaneous emission. Physics Reports. 1982;93(5):301-96.

[19] Cong K, Zhang Q, Wang Y, Noe GT, Belyanin A, Kono J. Dicke superradiance in solids [Invited]. JOSA B. 2016;33(7):C80-C101.

[20] Schuurmans MFH. Superfluorescence and amplified spontaneous emission in an inhomogeneously broadened medium. Optics Communications. 1980;34(2):185-9.

[21] Ariunbold GO, Sautenkov VA, Scully MO. Temporal coherent control of superfluorescent pulses. Optics Letters. 2012;37(12):2400-2.

[22] Rastegari A, Diels JC, Kamer B, Liu LR, Arissian L. Measurement of delayed fluorescence in N2+ with a streak camera. Optics Express. 2022;30(17):31498-508.

[23] Mattar FP, Gibbs HM, McCall SL, Feld MS. Transverse effects in superfluorescence. Physical Review Letters. 1981;46(17):1123.

[24] Maki JJ, Malcuit MS, Raymer MG, Boyd RW, Drummond PD. Influence of collisional dephasing processes on superfluorescence. Physical Review A. 2089;40(9):5135.

[25] Theer P, Kuhn B, Keusters D, Denk W. Two-photon microscopy and imaging. Neurobiology. 2005;77:5-2.

[26] Xu C, Zipfel W, Shear JB, Williams RM, Webb WW. Multiphoton fluorescence excitation: new spectral windows for biological nonlinear microscopy. Proceedings of the National Academy of Sciences. 1996;93(20):10763-8.

[27] Kang D, Zhu S, Liu D, Cao SE, Sun M. One-and Two-Photon Absorption: Physical Principle and Applications. The Chemical Record. 2020;20(9):894-911.

[28] Demtröder W. Laser Spectroscopy: Vol. 1 Basic Principles. Springer; 2008.

[29] Demtröder W. Laser Spectroscopy: Vol. 2 Experimental Techniques. Springer; 2008.

[30] Perez-Arjona I, de Valcárcel GJ, Roldán E. Two-photon absorption. Revista Mexicana de Física. 2003;49(1):92-101.

[31] Stancu GD. Two-photon absorption laser induced fluorescence: rate and density-matrix regimes for plasma diagnostics. Plasma Sources Science and Technology. 2020;29(5):054001.

[32] Polynkin P, Cheng Y. Air lasing. vol. 208. Springer; 2018.

[33] Kuan YH, Liao WT. Transition between amplified spontaneous emission and superfluorescence in a longitudinally pumped medium by an x-ray free-electron-laser pulse. Physical Review A. 2020;101(2):023836.

[34] Kornienko V, Bao Y, Bood J, Ehn A, Kristensson E. The space-charge problem in ultrafast diagnostics: an all-optical solution for streak cameras. Ultrafast Science. 2024;4:0055.

[35] Kinefuchi K, Nunome Y, Cho S, Tsukizaki R, Chng TL. Two-photon absorption laser induced fluorescence with various laser intensities for density measurement of ground state neutral xenon. Acta Astronautica. 2019;161:382-8.

[36] Eichhorn C, Fritzsche S, Löhle S, Knapp A, Auweter-Kurtz M. Time-resolved fluorescence spectroscopy of two-photon laser-excited 8 p, 9 p, 5 f, and 6 f levels in neutral xenon. Physical Review E. 2009;80(2):026401.